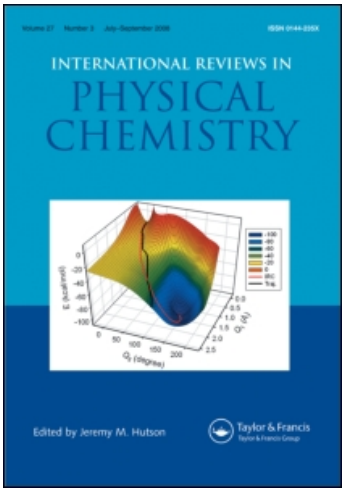

International Reviews in Physical Chemistry
Publication details, including instructions for authors and subscription information:
http://www.informaworld.com/smpp/title~content=t713724383

Metal-ligand interactions: Gas-phase transition metal cluster carbonyls

Kent M. Ervin[a]
[a] Department of Chemistry and Chemical Physics Program, University of Nevada, Reno, NV, USA

Online publication date: 26 November 2010

To cite this Article Ervin, Kent M.(2001) 'Metal-ligand interactions: Gas-phase transition metal cluster carbonyls', International Reviews in Physical Chemistry, 20: 2, 127 — 164
To link to this Article: DOI: 10.1080/01442350010028532
URL: http://dx.doi.org/10.1080/01442350010028532

INT. REVIEWS IN PHYSICAL CHEMISTRY, 2001, VOL. 20, NO. 2, 127–164

Metal–ligand interactions: gas-phase transition metal cluster carbonyls

KENT M. ERVIN†

Department of Chemistry and Chemical Physics Program, University of Nevada, Reno, NV 89557, USA

Experimental studies of the interactions of small transition-metal cluster anions with carbonyl ligands are reviewed and compared with neutral and cationic clusters. Under thermal conditions, the reaction rates of transition-metal clusters with carbon monoxide are measured as a function of cluster size. Saturation limits for carbon monoxide addition can be related to the geometric structures of the clusters. Both energy-resolved threshold collision-induced dissociation experiments and time-resolved photodissociation experiments are used to measure metal–carbonyl binding energies. For platinum and palladium trimer anions, the carbonyl binding energies are assigned to different geometric binding sites. Platinum and palladium cluster anions catalyse the oxidation of carbon monoxide to carbon dioxide in a full catalytic cycle at thermal energies.

Contents

† Email: ervin@chem.unr.edu

International Reviews in Physical Chemistry ISSN 0144-235X print/ISSN 1366-591X online © 2001 Taylor & Francis Ltd
http://www.tandf.co.uk/journals
DOI: 10.1080/01442350010028532

1. Introduction

The active centres in supported metal catalysts used for industrial processes are often small crystallites (1–50 nm) [1]. Smaller metal clusters on supports have also been synthesized as catalysts [2]. Experiments using mass-selective deposition of platinum clusters on a magnesium oxide substrate for the oxidation of carbon monoxide (CO) have recently demonstrated a monodisperse supported catalyst showing size-selective catalytic activity [3]. Although bulk gold surfaces are relatively inert, nanometre sized gold particles show catalytic activity [4]. Gas-phase metal clusters thus serve as interesting model systems for fundamental studies of catalytic processes. Gas-phase metal clusters also can themselves be catalysts [5, 6]. For example, CO can be catalytically oxidized to carbon dioxide (CO_2) with nitrous oxide (N_2O) or oxygen (O_2) using platinum cluster anions in a full catalytic cycle under near room-temperature conditions [6].

Modern research into gas-phase metal clusters began with the development in the early 1980s of laser vaporization sources to make beams of metal clusters [7, 8]. Exploratory studies of cluster reactivity soon followed [9, 10]. For some metal cluster systems, reactivities show strong variation with cluster size, implying a promise of 'size-selective' chemistry [11–13]. Many transition-metal cluster properties (e.g. ionization energies [14, 15], electron affinities [16–20], dissociation energies [21–25] and magnetic properties [26]) have been measured as a function of size, probing the transition from molecular properties at small sizes to the bulk limit. These quantitative measurements provide benchmarks for theoretical electronic structure calculations, which are increasingly applied but remain challenging for transition-metal species. Reactivity studies continue to provide intriguing information about size-selective transition-metal cluster chemistry [5, 6, 9–13, 27–48].

A frustration in cluster science has been the unavailability of structures of gas-phase metal cluster species. Except for small sizes or highly symmetric species, the rovibronic spectra of open d-shell transition metal clusters tend to be too complicated and congested to provide direct structural information, but progress is being made in experimental spectroscopy [49–57] and theory [58] of both small bare metal clusters and clusters with ligands or adsorbates. There is now some hope for obtaining detailed structural information for clusters with more than a few metal atoms, the lack of which has limited understanding the chemical reactivity of clusters in terms of structure–reactivity relationships. A combination of theory and experimental spectroscopy has provided firm geometric assignments for some small species including Nb_3O^- [51], Nb_3N_2 [52], Nb_3C_2 [53], Ag_5 [54] and Ag_7 [55]. Infrared photodissociation spectra of metal clusters with adsorbed molecules have provided information about the metal–ligand interactions [50, 56, 57]. $Fe_4(CO)_{14}$ was prepared in by cryogenic matrix isolation by co-condensation of mass-selected Fe_4^+ clusters with CO and studied by infrared spectroscopy, but the structure could only be partially assigned [46]. Geometries remain uncertain for most large or complex transition metal cluster systems. Cluster scientists have relied on chemical and physical properties of the clusters to make inferences of their geometric and electronic structure. Chemisorption patterns, for example, can be used to probe metal cluster structures [59–64].

A number of reviews have appeared examining various aspects of metal cluster research [65], including neutral transition-metal and main group clusters [13, 66–69], metal and semiconductor cluster ions [27, 70], photodissociation of metal cluster ions [22], photoelectron spectroscopy of metal cluster anions [16, 20], quantum size effects in nanometre-scale metal clusters [71], synthesis and catalytic applications of transition-

metal nanoclusters in solution [72], reactions [13, 73, 74] and spectroscopy [49, 50] of neutral transition-metal clusters, thermochemistry of transition-metal clusters [30] and metal–ligand systems [75], spectroscopy of transition-metal dimers [67, 76] and theoretical treatments of metal clusters [58]. This review focuses on illustrative aspects of our metal cluster work at the University of Nevada, Reno, over the past decade. Primarily, the interactions of transition-metal cluster anions with CO are discussed with comparisons with other work in the field. Because a majority of the work in the field of transition-metal clusters is on neutral and cationic species, examining anions can help to distinguish effects due to the total charge, the number of atoms in the cluster or the number of valence electrons. For the present purposes, the copper-group elements are included among the transition metals.

Metal cluster carbonyls serve as a case study of the information that can be obtained about metal–ligand or metal–absorbate interactions from gas-phase cluster studies. CO is an interesting reactant molecule for cluster studies because a great deal of information is available about CO adsorbed on metal crystal surfaces [77, 78] and about carbonyls in organometallic complexes in the condensed phase [79–82]. Metal–carbonyl interactions are important in practical catalytic processes, for example in the oxidation of CO to CO_2 in automotive catalytic converters [83]. The nature of the bonding between CO and transition-metal centres has been studied extensively theoretically [84, 85]. The Blyholder [86] model is the generally accepted view of the bonding of CO to metal centres. The lone-pair σ electrons on CO donate into an empty metal orbital, while occupied π or δ orbitals on the metal back-donate into the π^* antibonding orbital on CO. The relative strength of the σ donation and π back-bonding interaction has been the subject of much discussion and depends on the details of the orbital overlaps.

2. Transition-metal cluster production

The pulsed laser and pulsed helium vaporization source for metal clusters designed by Smalley and co-workers [7] has been adapted or modified for a variety of purposes including ionic clusters and continuous or pseudocontinuous operation [8, 87–92]. Fast-atom and secondary-ion sputtering also produce metal clusters [93–96], although these processes tend to produce internally excited ions. A pulsed arc discharge source [97, 98] is similar to the laser vaporization source but with the ablation energy provided by an electrical discharge.

2.1. *Metal cluster discharge source*

In our work, metal cluster anions are produced in an ion flow tube reactor [99] by a dc discharge source of the type developed by Lineberger and co-workers [100, 101]. Our ion flow tube reactor instrument [99] is shown in figure 1. A cathode fabricated from the metal of interest, or covered by a metal foil, is located at the centre of the flow tube near its upstream end. The water-cooled cathode is placed at between -1 and -3 kV relative to the grounded flow tube, creating a discharge plasma in the buffer gas composed of helium with 5–10% argon at a total pressure of 0.2–0.6 Torr. The discharge draws a current of typically a few milliamperes. Metal clusters are produced when argon or other cations are accelerated to the cathode and sputter the metal surface. Many neutrals are produced, as shown by the deposition of metal on the walls of the flow tube, and some anionic clusters are produced, either directly or by electron

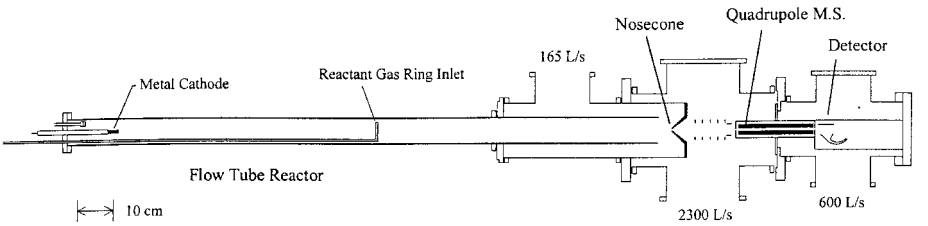

Figure 1. Ion flow tube reactor with dc discharge metal cluster source and quadrupole mass spectrometer (M.S.) detector.

attachment to neutral species in the plasma. There is no evidence of significant clustering downstream of the discharge region [101]. The clusters are thermalized by 10^4–10^5 collisions with the room-temperature buffer gas during their residence time of about 5 ms in the flow tube. Photoelectron spectroscopy of metal clusters formed by the ion flow tube discharge source shows that the internal vibrational temperatures are near the buffer gas temperature [101, 102].

Figure 2 shows mass spectra of copper-group cluster ions produced by the dc discharge source. The cluster size intensity distributions peak at two to five atoms, with usable intensities up to 15 atoms depending on the metal. Advantages of the discharge cluster source are that it is inexpensive, it produces intense cluster beams for most transition-metal elements and the clusters are well thermalized. Another advantage of the ion flow tube reactor source is that reagent molecules can be introduced downstream of the discharge to induce ion–molecule reactions under controlled thermal laminar flow conditions. This feature is used to synthesize cluster–ligand adduct ions for beam experiments and can also be used for reaction kinetics measurements as discussed below. Compared with laser vaporization, the cluster sizes produced by the dc discharge source tend to be smaller. Only anionic clusters are produced; the same source design makes atomic transition-metal cations [103], but not significant quantities of cationic metal clusters [104].

2.2. *Cluster intensity distributions and 'magic numbers'*

Intensity anomalies in mass spectra from a cluster source (so-called 'magic numbers') are often attributed to the stability of certain cluster sizes [105, 106]. Alkali metal clusters (whose atoms have s^1 valence electron configurations), for example, exhibit distinct steps at electronic shell closings predicted by the jellium model for spheroidal clusters with 2, 8, 18, 20, ... electrons [107–109]. Buckminsterfullerene (C_{60}) is a famous example of an important new species discovered by its appearance as a magic number in the mass spectrum of carbon clusters [110]. In general, however, mass spectral intensities are ambiguous indicators of thermodynamic stability because they may be controlled by kinetic factors in the cluster source, often under poorly characterized conditions. Metastable isomers of clusters may also be produced, which can sometimes be detected and removed by post-source annealing [111] or identified by spectroscopic or reactivity measurements [112–114].

The mass spectra of copper-group clusters [115] shown in figure 2 illustrate the ambiguities of interpreting mass spectral intensities. Copper, silver and gold atoms have a $d^{10}s^1$ valence configuration. The electrons of the closed d shell remain mainly localized on the atoms in the clusters, while the single s valence electron is involved in the bonding. Thus, copper-group clusters exhibit 'alkali-like' behaviour and are

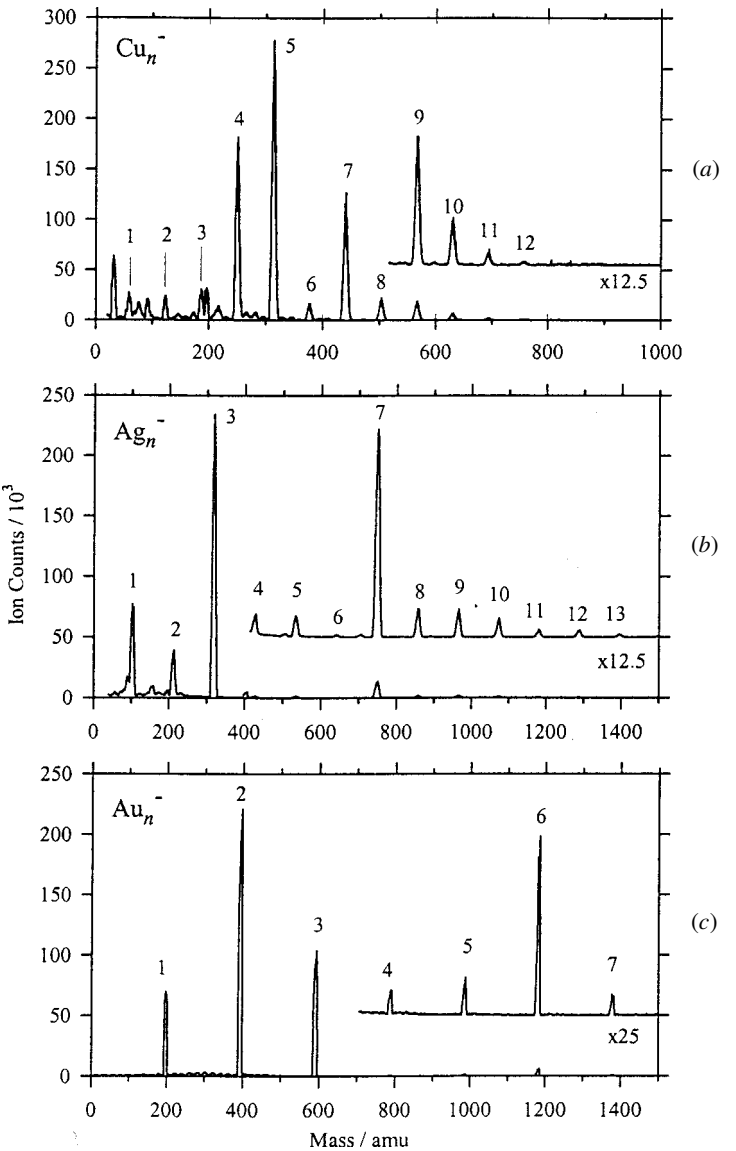

Figure 2. Mass spectra of (*a*) copper, (*b*) silver and (*c*) gold cluster anions produced by the dc discharge cluster source.

qualitatively consistent with the jellium model in the size dependence of ionization potentials [116–119], electron affinities [18, 19, 100, 101] and dissociation energies [24, 25, 120–125]. For the small cluster anions, the M_7^- clusters with eight valence electrons exhibit special stability, that is high electron binding energies and dissociation energies relative to neighbouring cluster sizes [25, 101, 124, 125]. In our mass spectra of the copper and silver cluster anions (figure 2), Cu_n^- and Ag_n^- with $n = 7$ (eight valence electrons) exhibit stronger intensities relative to at least $n = 6$ and $n = 8$ but, for gold clusters, Au_6^- with seven valence electrons is significantly and reproducibly more intense than its neighbours. This behaviour is *not* matched by quantitative measurements of the electron affinities and dissociation energies of gold clusters, for which the

eight-electron species show higher stability than neighbouring sizes [19, 120]. Thus, the 'magic' intensity of Au_6^- must be attributed to kinetic effects in the discharge source, rather than to its thermochemical stability. Vibrational autodetachment spectroscopy [126] and early theoretical calculations [127] on Au_6^- suggested a symmetric planar D_{6h} hexagonal ring structure, although zero-electron-kinetic-energy photoelectron spectroscopy suggests that the anion geometry may be distorted [128] and recent calculations show a planar D_{3h} triangular structure [129]. Larger cluster anions probably have three-dimensional structures rather than planar structures [129]. Thus, a kinetic bottleneck in the discharge source for the growth of nonplanar structures from smaller planar structures might explain the anomalously high intensity of Au_6^- even though it is not most stable thermodynamically.

3. Transition-metal cluster reactivity

The reactivity of metal clusters has been characterized by various experimental methods, including fast flow reactor kinetics in the post-vaporization expansion region of a laser ablation source [14, 130], ion flow tube reactor kinetics of ionic clusters [99, 131], ion cyclotron resonance [42, 91, 132] and guided-ion-beam experiments [6, 21, 133]. These techniques are distinguished by the charge state of reactants (neutral, cationic or anionic), by whether the clusters are size selected before the reaction zone, by single or multiple collisions of the clusters with the reactant molecules, by the pressure of a buffer gas if present, and by the temperature and collision energy of the reactants.

Our ion flow tube reactor [99] (figure 1) has been used for reaction rate coefficient and product distribution measurements. The use of flow tube reactors (flowing afterglow) for kinetic measurements has been thoroughly reviewed [134]. Similar kinetics measurements on neutrals can be made using the post-ablation flow region in a laser vaporization source [14, 130], but often the flows, pressures, concentrations and detection efficiency are less well characterized so only relative reaction rates are obtained. Measurements of absolute thermal rate coefficients of metal cluster ions are routine with the ion flow tube reactor method [99, 131, 134]. Our analysis procedures have been described in detail [99].

3.1. *Carbonyl addition reaction rates*

We have used the ion flow tube reactor method to examine the reactions of copper-group [115], nickel-group [99, 135], niobium [136] and cobalt [59] cluster anions with CO, as well as with other small neutral reactant species [59, 115, 136, 137]. For example, figure 3 shows kinetic data for the reactions of platinum cluster anions with CO. The cluster ion intensities are depleted as the CO concentration is increased. Treating the kinetics as pseudo-first-order [99], the slopes of these plots yield the effective bimolecular rate coefficients for

$$M_n^- + CO \rightarrow \text{products} \qquad (1)$$

where in this case M = Pt. The primary product channel is simple addition of CO to the intact metal cluster anions. Figure 4 compares the effective bimolecular rate coefficients for reactions of CO with copper, gold, cobalt, niobium, nickel, palladium and platinum cluster anions [59, 15, 135, 138]. The addition reaction results from the

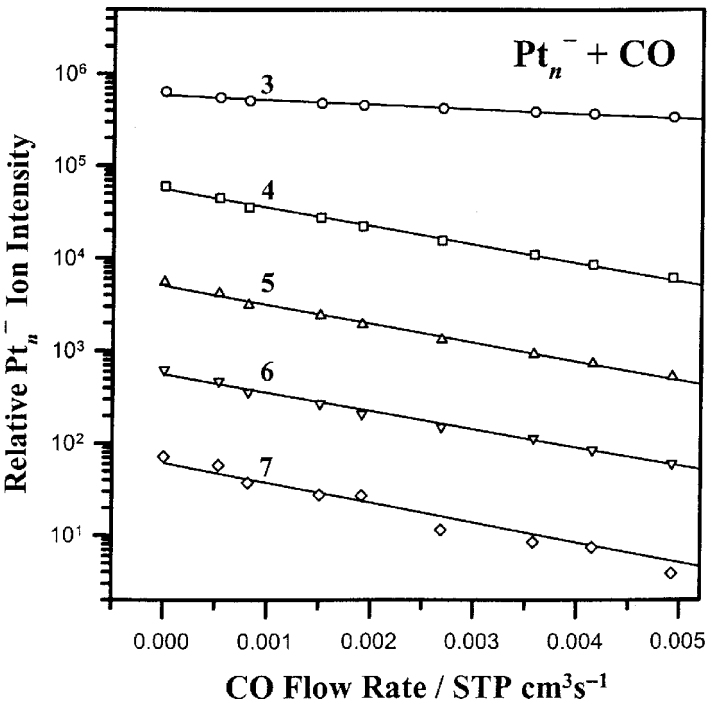

Figure 3. Kinetic data for the reaction of platinum cluster anions with CO in the ion flow tube reactor under pseudo-first-order conditions. Relative intensities of the platinum clusters are plotted as a function of CO flow rate (proportional to concentration) at a helium buffer gas pressure of 0.45 Torr. The lines are linear regression fits with slopes proportional to the effective bimolecular rate coefficients for total depletion of each cluster.

stabilization of the nascent cluster–carbonyl complex by buffer gas collisions. The effective bimolecular rate constants in figure 4 are for a buffer gas pressure of about 0.45 Torr. For each element, the rates show a general increase with increasing cluster size, with only minor oscillations as a function of size. Effective bimolecular rate coefficients for the addition of CO to Ni_n^- (n = 3–10), Pd_n^- (n = 3–8), and Pt_n^- (n = 3–7) range from about 10% of the collision rate for the trimer anions to more than 70% of the collision rate for clusters larger than four atoms, which is consistent with the high sticking coefficients for CO scattering from the bulk metal surfaces [139–141]. The reaction with niobium cluster anions is also near the collision rate for $n > 3$. Cobalt cluster anions appear to approach the collision rate more slowly with increasing size. The high reaction efficiencies in the gas phase and the high sticking coefficients on surfaces can both be attributed to the strong interaction of CO with the metal centres for open d-shell transition metals.

As shown in figure 4, copper-group clusters are relatively unreactive compared with nickel-group, cobalt and niobum clusters. Copper and gold cluster anions react with CO by addition, with effective rate coefficients shown in figure 4, but silver cluster anions are completely unreactive with CO under the flow tube reactor conditions [115], as are silver dimers [142]. The low reactivity can be attributed [115] to the stability of the full d-electron shell in the copper group, which makes π back bonding unfavourable. The d-shell orbitals lie at lower energies relative to the s electrons for silver than for copper or gold. There is at most a slight even–odd alternation in

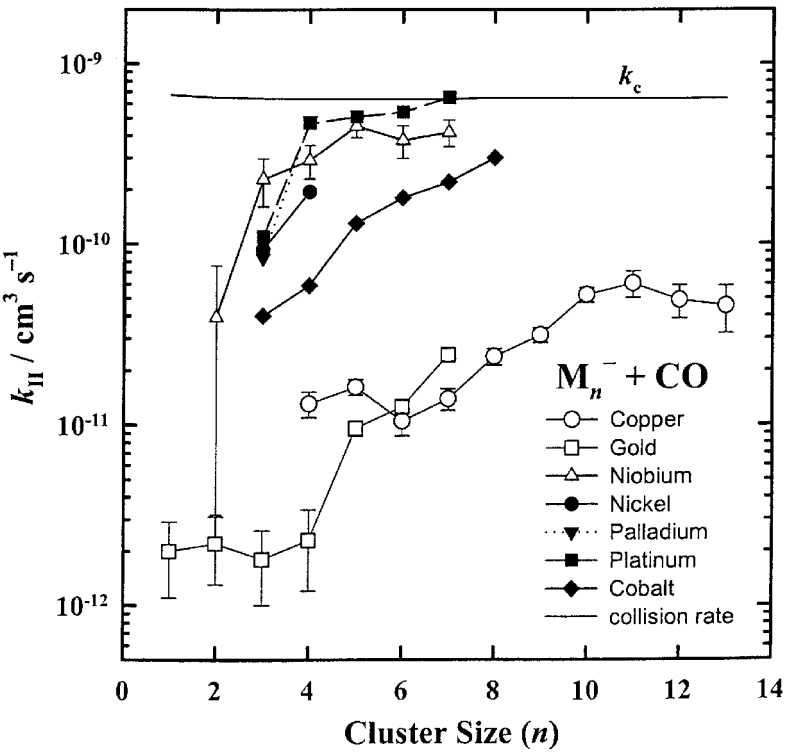

Figure 4. Effective bimolecular rate coefficients for the reactions of cobalt, copper, gold, nickel, niobium, palladium and platinum cluster anions with CO at a buffer gas pressure of approximately 0.45 Torr. The primary initial reaction is addition of CO in each case. No reaction was observed for silver cluster anions with CO. The line labelled k_c is the collision rate constant for the ion–dipole potential (neglecting small reduced-mass differences that are barely discernible on this scale).

reaction rates of the copper and gold cluster anions with CO, in contrast with strong even–odd alternation of the rates with O_2 [115]. This behaviour is consistent with the idea that the reverse dissociation of CO from the clusters is a heterolytic dissociation process that should have no potential energy barrier on molecular orbital grounds [143]. In contrast with CO as a two-electron donor, O_2 interacts attractively or repulsively with the filled (odd n) or half-filled (even n) highest occupied molecular orbital (HOMO) of the cluster anion respectively, through the unpaired electron in an O_2 π^* antibonding orbital. This interaction gives rise to the even–odd alternation in reactivity with O_2.

The metal clusters that react with CO near the collision rate, for example niobium and platinum cluster anions of sizes greater than four or five atoms, tend to show no buffer gas pressure dependence over the 0.2–0.6 Torr range accessible in the flow tube reactor. In contrast, small copper and gold cluster anions, with much lower reaction efficiencies, have effective bimolecular reaction rates that are dependent on the buffer gas pressure [115]. Figure 5 shows the pressure dependence of the apparent bimolecular reaction rate coefficients of reaction (1) for copper and gold cluster anions. The y intercepts of these plots yield the true bimolecular rate coefficient, and their slopes are proportional to the third-order association rate coefficient k_{III} for

$$M_n^- + CO + He \rightarrow M_nCO^- + He. \quad (2)$$

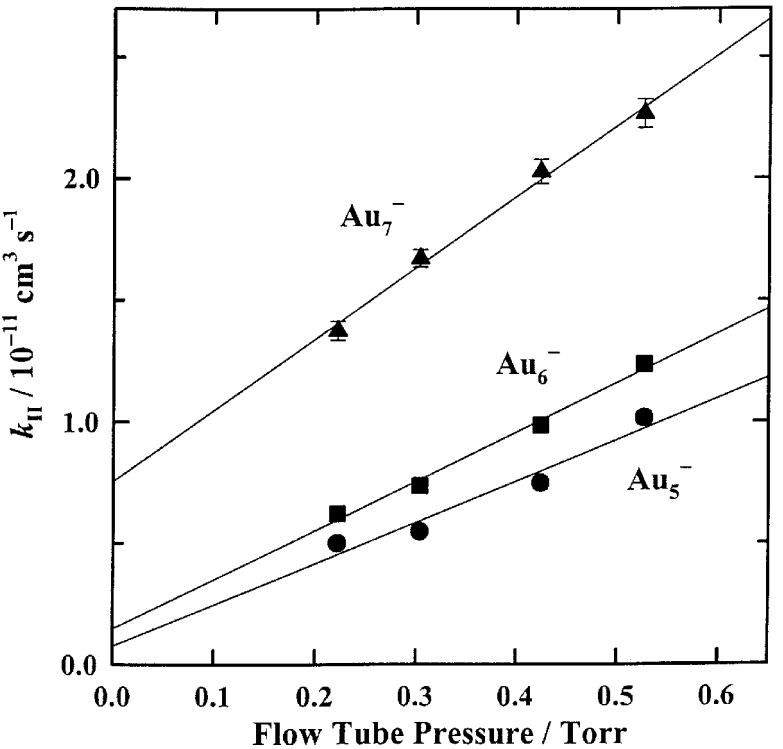

Figure 5. Pressure dependence of the apparent bimolecular rate coefficients for reaction of Au_n^- (n = 5, 6, 7) with CO. The lines are a linear regression fit. The slopes are proportional to the third-order association rate constant and the y intercept is the true bimolecular rate coefficient (in the absence of buffer gas collisions).

The probability of forming stable carbonyl association products increases with increasing buffer gas pressure [115], as can be explained by a simple Lindemann mechanism (3).

$$\begin{aligned} M_n^- + CO &\rightleftharpoons [M_nCO^-]^* \\ [M_nCO^-]^* + He &\rightarrow M_nCO^- + He. \end{aligned} \qquad (3)$$

If the lifetime of the nascent intermediate $[M_nCO^-]^*$ is shorter than or similar to the average time between collisions with the buffer gas, then the apparent bimolecular reaction rate for formation of M_nCO^- will depend on the buffer gas density. The observation of pressure-dependent effective bimolecular rate coefficients (figure 5) emphasizes that observed reaction rates and product distributions depend on the reaction conditions as well as on the intrinsic reactivities of the clusters.

Using the Lindemann model (3), the lifetimes of the metal cluster–carbonyl complexes can be calculated from the third-order association rate constants, as described in detail elsewhere [115]. The lifetimes extracted from the pressure-dependence data for carbon monoxide addition to small copper and gold cluster anions are shown in figure 6. The logarithmic dependence on cluster size or vibrational degrees of freedom is consistent with simple statistical models for the case that the CO binding energies have the same order of magnitude for all these cluster species [115].

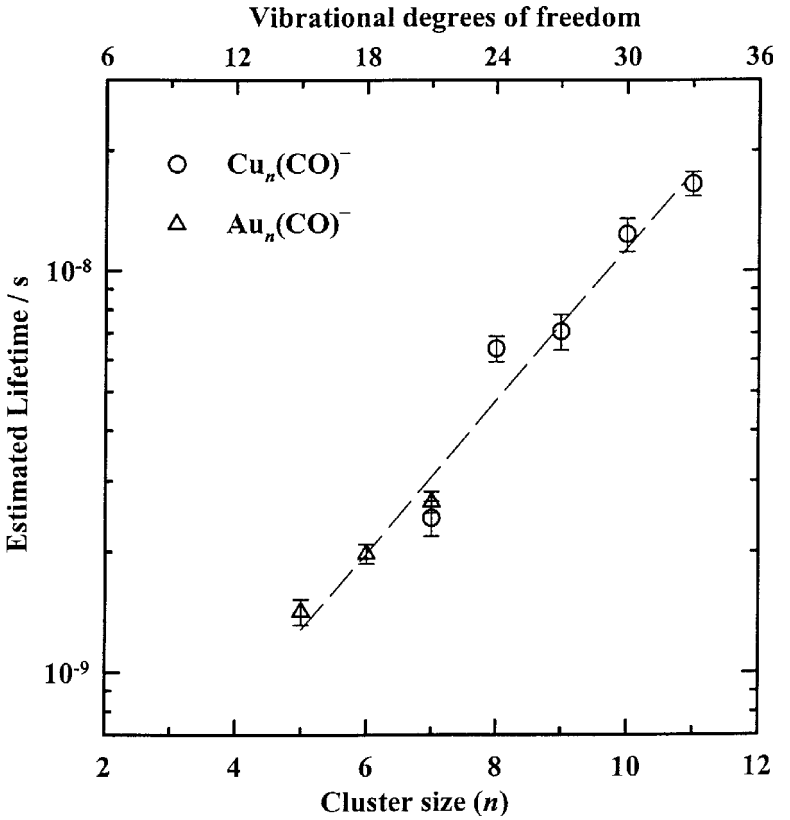

Figure 6. Estimated lifetimes of nascent $M_n(CO)^-$ complexes in M^-_{nm} + CO collisions, obtained using the Lindemann mechanism model from measured association rate constants.

Small cobalt cluster anions show CO addition rates that are intermediate between the fast rates for nickel-group clusters and slow rates for copper-group clusters (figure 4). Unlike most copper- and nickel-group cluster anions, some cluster fragmentation is observed as carbonyls are initially adsorbed, which can be explained by higher CO adsorption energies for cobalt [59]. This behaviour reflects a balance between the lifetime of the initial complex against statistical decomposition and the frequency of stabilizing buffer gas collisions. The complexes of the larger clusters have longer unimolecular decomposition lifetimes, increasing the effective addition probability. Platinum clusters also have strong affinities for carbonyls, but the metal—metal bonds are relatively stronger than for cobalt clusters. These factors increase the lifetimes of the initial complexes and thereby the stabilization probability, making fragmentation less favourable upon carbonylation.

3.2. *Product distributions and saturation limits*

In addition to reaction rates, we have measured product distributions and adsorption saturation limits [59, 135–137]. Under our flow tube reactor conditions, multiple CO molecules can add to the transition-metal cluster anions after the initial addition reaction:

$$M_n(CO)^-_m + CO \rightarrow M_n(CO)^-_{m+1}. \quad (4)$$

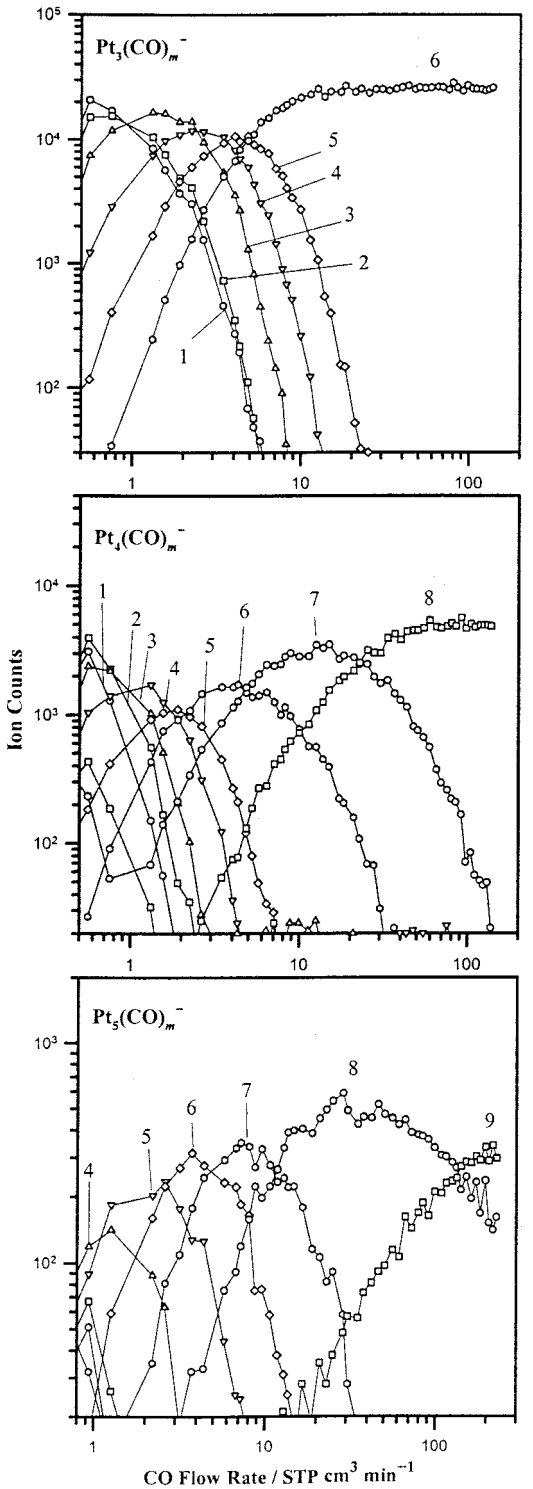

Figure 7. Product ion intensities for the reactions Pt_n^- (n = 3, 4, 5) with CO as a function of CO flow rate in the ion flow tube reactor.

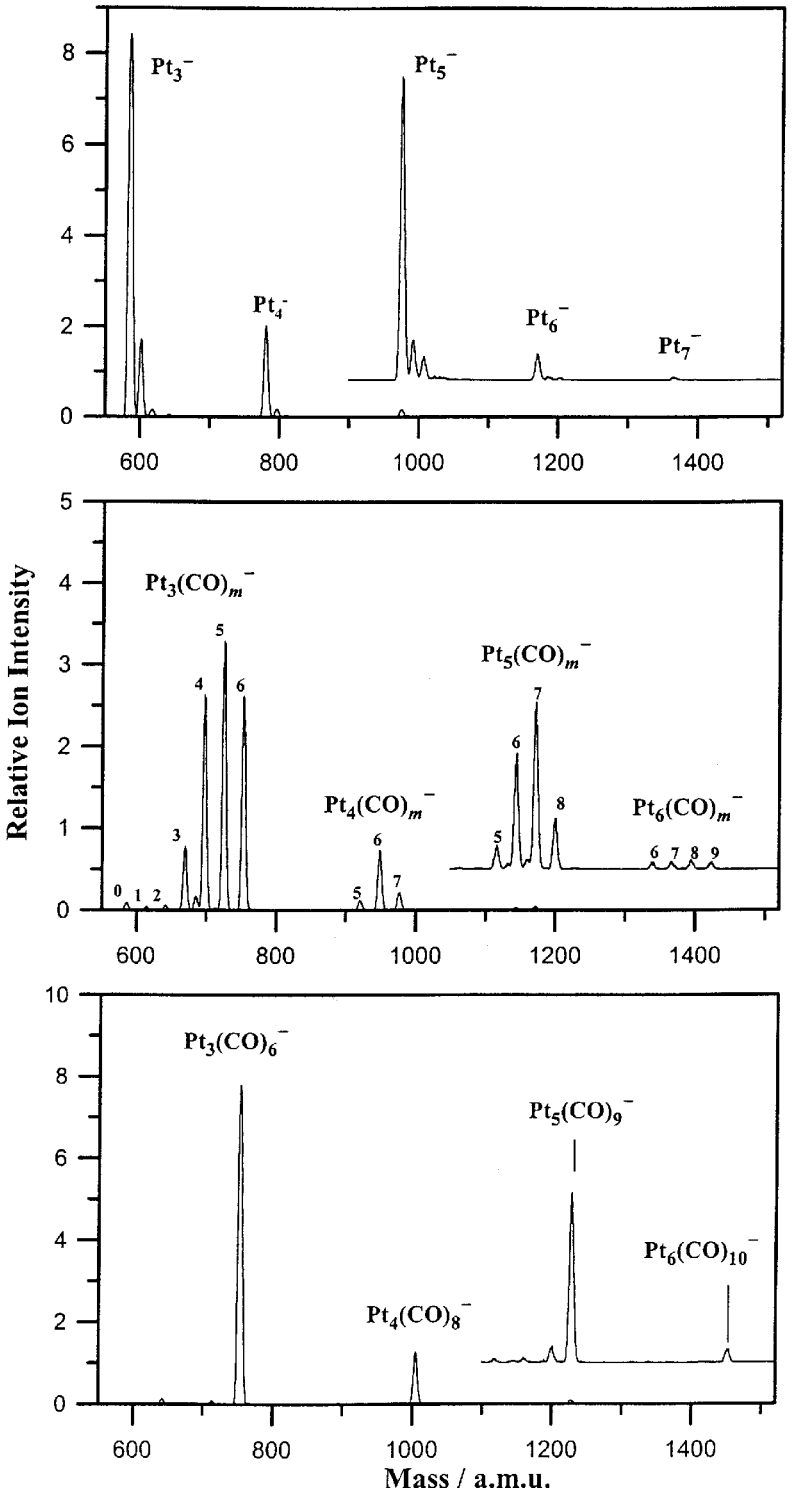

Figure 8. Mass spectra of platinum cluster anions and carbonyl addition products from the ion flow tube reactor with (*a*) no CO reactant gas, (*b*) a moderate flow rate of CO and (*c*) a high flow rate of CO. The labelled peaks in the bottom spectrum represent the saturation limits.

Figure 7 shows product ion intensities for additions of CO to small platinum cluster anions Pt_n^- (n = 3–5) as a function of the flow rate of CO introduced into the flow tube at a point downstream of the cluster ion source [99]. These plots show that CO adds to the clusters in a sequential manner. For platinum cluster anions, the reaction rates for sequential additions of CO are rapid and fairly uniform, without major intermediate bottlenecks, up to a saturation limit that depends on the size of the cluster. In figure 7, the saturation limit is clearly shown as m = 6 carbonyls for Pt_3^- and m = 8 for Pt_4^-, but saturation is less obvious for Pt_5^-. Because of the limited reaction time in the flow tube reactor, it is difficult to achieve full saturation for larger clusters under well-controlled kinetic conditions. Figure 8 shows mass spectra [99] of the platinum cluster anions with no CO, at an intermediate flow rate of CO, and with an extremely high flow rate of CO. The latter plot clearly shows saturation limits of m = 9 for Pt_5^- and m = 10 for Pt_6^-. Thus, a combination of kinetics and mass spectrometry measurements can determine the saturation limits with reasonable certainty, although it is possible that more extreme conditions can cause rearrangements, leading to higher saturation [48].

We have made measurements of CO saturation limits on platinum [99], nickel, palladium [135] and cobalt [59] cluster anions. Carbonyl saturation limits could not be obtained for the copper-group cluster anions [115] because of their low reactivities; only one to three CO molecules are observed to add to the clusters and it is not completely clear whether these are saturation limits or are kinetically limited. For niobium cluster anions [136], the sequential CO addition rates are rapid, but the niobium systems are subject to a greater degree of fragmentation of the metal cluster core. This behaviour, which is attributed to the high CO binding energies on early transition metals [77], leads to a number of fragmentation products, which then also add carbonyls in a complicated pattern.

The conversion from bare cluster anions to clusters with the same number of metal atoms but saturated with CO is near 100% for the nickel-group cluster anions ($n >$ 3), that is no fragmentation occurs. The high observed conversion efficiency indicates that the M_n^-–CO binding energy is less than the M_n^-–M binding energies, as is expected from bulk values. While the initial rates for adsorption of the first CO are all fast for large nickel-group clusters, the rates of sequential addition varies for various cluster sizes and for the three metals. Platinum clusters go quickly to saturation, while intermediate bottlenecks are found for some nickel and palladium cluster anions.

The palladium cluster carbonyl anions that we observe [135] represent the first examples of saturated binary (homoleptic) palladium carbonyl compounds. Unsaturated gas-phase $Pd_n(CO)_{1-3}$ species have been observed in fast-flow reactor metal cluster sources [130]. Attempts to synthesize binary palladium carbonyl compounds in solution have not been successful [80], which implies that palladium carbonyl complexes may be unstable or reactive. Palladium carbonyl compounds have been prepared in cryogenic matrices [144] and as a surface film grown on alumina below 190 K [145], but these decompose or lose carbonyls at higher temperatures. Solution-phase palladium carbonyl complexes can be prepared using other stabilizing ligands [146], and CO readily adsorbs on palladium surfaces [147]. Our ability to make saturated palladium cluster carbonyl as easily as for the corresponding nickel and platinum clusters indicates that the synthetic difficulty is not due to intrinsic instability of the palladium carbonyls, but perhaps is due to higher reactivity with other reactants or other kinetic effects.

3.3. *Saturation limits versus structure*

For saturation limits to be related to the structure of the bare metal cluster anion, it must be assumed that the skeletal structure does not undergo rearrangement upon adsorption. The observation of fragmentation upon carbonylation for the niobium cluster anions [136] shows that rearrangements can occur. Therefore, relationships between the saturation limits and the skeletal structure of the metal clusters strictly only applies to the final saturated species. However, for the nickel-group cluster anions, the CO binding energies are expected to be smaller than the metal–metal binding energies. This will limit the possibility of rearrangements. Under our flow tube conditions, the ions undergo about 10^3 collisions with the buffer gas for each reactive encounter with CO. Thus, most of the energy gained by addition of one CO will be removed from the cluster before another CO adds to it, at least for small cluster sizes.

There are three basic approaches to using adsorption patterns and saturation limits to determine metal cluster structures. The first approach is to count the number and type of adsorption sites and then to compare this with possible geometric structures for a given cluster size. Experiments of this type have been used to determine structural features of large neutral transition-metal clusters [47, 48, 64, 106, 148–159]. For this approach to be valid, the adsorbate molecule must predominantly adsorb at a site of a single geometry. The second approach is to use electron-counting rules from organometallic chemistry to relate the total number of cluster valence electrons to the skeletal structure of the clusters [60, 62, 99, 135, 160–162]. Electron-counting rules are derived from molecular orbital considerations and the propensity for most transition metals to complete an 18-electron valence shell either from donation of electrons from ligands or by sharing electrons in metal—metal bonds. Relatively simple rules [163–169] successfully rationalize the structures of many organometallic cluster compounds, as determined by X-ray crystallography or other structural tools. Electron-counting rules are appropriate when the electron molecular orbital structure for the whole cluster, rather than localized metal–ligand interactions, are the controlling factor. For small transition-metal cluster carbonyls, the electron-counting approach is appropriate because CO is able to bind in several ways (terminal, edge bridging or face bridging) to accommodate the most stable electronic structure of the cluster and because the metal–metal distances are somewhat flexible (compared with the metal crystal lattice or large close-packed clusters). The third method, proposed by Parks *et al.* [47, 48], examines the number of ligands that can add to a cluster in a tight-packing limit. If the ligand is completely undiscriminating with regard to binding site, then the saturation coverage limit is controlled by how close the ligands can be packed over the cluster surface, which in turn depends on the surface area of various geometric structures. In experiments on the binding of CO to neutral nickel clusters, Parks *et al.* [47, 48] found that saturation limits were consistent with the tight packing using van der Waals radii for the sizes of the CO ligands and the bulk lattice value for the Ni–Ni distances. None of these three methods provides structures for clusters that are as definitive as spectroscopy measurements could be where feasible. That is fundamentally because for large clusters there is bound to more than one structural isomer that gives the same number of binding sites or the same number of valence electrons.

For small transition-metal cluster anions saturated with carbonyls, we have applied electron-counting rules to examine cluster structures. The cobalt clusters [59] are illustrative. Carbonyls are observed to add sequentially to the cobalt cluster anions up to a saturation limit, despite minor fragmentation and intermediate bottlenecks. We can use electron-counting schemes to identify the possible skeletal structures of the

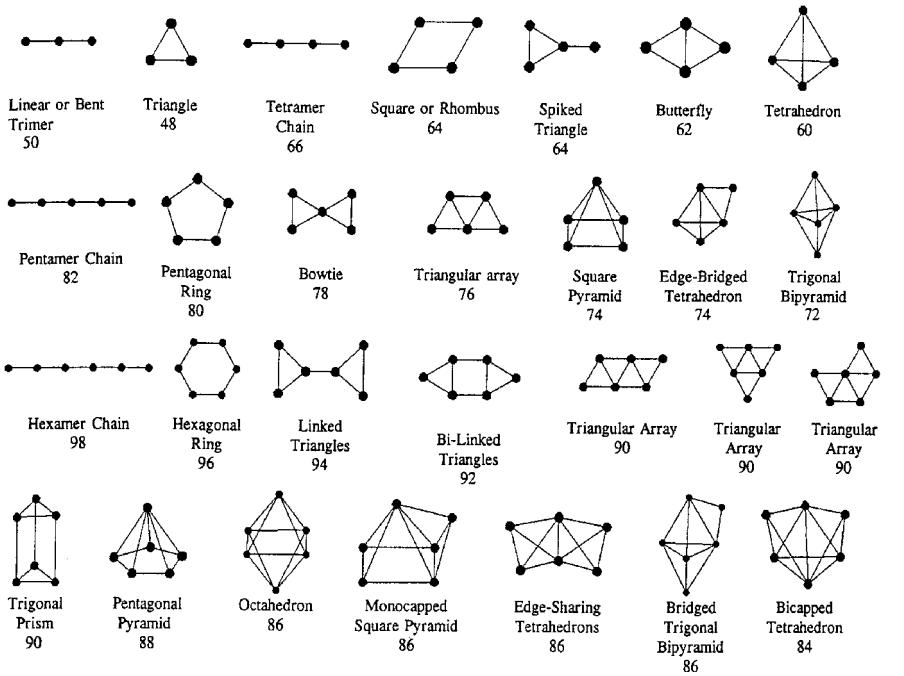

Figure 9. Total number of cluster valence electrons (number below each structure) for metal clusters of various sizes (n = 3–6) and skeletal geometries as predicted by PSEPT (see text).

saturated species. With several exceptions, the total valence electron counts are consistent with those observed by Castleman and co-workers [60] for cobalt cluster cations saturated with CO. For example, the saturation limit for the cobalt pentamer anion is $Co_5(CO)_{13}^-$ with 72 cluster valence electrons (counting nine electrons for each s^2d^7 cobalt atom, two electrons donated by each carbonyl and one for the extra charge). The corresponding saturated cationic cluster is $Co_5(CO)_{14}^+$, which also has 72 cluster valence electrons (CVEs). According to the polyhedral skeletal electron pair theory (PSEPT) [169], a pentanuclear metal complex with 72 CVEs corresponds to a trigonal bipyramidal skeletal structure. For the hexamer, the saturated species [59, 60] are $Co_6(CO)_{13}^-$ and $Co_6(CO)_{16}^+$, each with 85 CVEs. The odd number of electrons results from having singly charged species in the gas phase; in solution, solvation can stabilize multiply charged ions. We interpret the saturation limit as meaning that the cluster valence orbitals cannot accept another two electrons from an additional carbonyl; thus, 85 CVEs corresponds to 86 CVEs for a closed-shell species in solution. The cobalt hexamers can be compared with other metals. The saturated nickel and palladium hexamer anions, $M_6(CO)_{12}^-$ (M = Ni or Pd) also possess 85 CVEs [135], and Wöste and co-workers [161, 162] found a saturation limit of $Ni_6(CO)_{13}^+$ (85 CVEs) for the cationic nickel hexamer. The saturated platinum hexamer anion is $Pt_6(CO)_{10}^-$ (81 CVEs), but platinum is known to be electron deficient compared with the 18-electron closed shell because of the high-lying p orbitals for the late third-row transition metals [99, 135]. Thus, all these hexamer clusters are consistent with 86 CVEs for an 18-electron metal with a closed shell. For the cationic cobalt and nickel hexamers, these were assigned to an octahedral skeletal structure [60, 61]. However, a careful examination [99] of all possible structures shows that PSEPT predicts that four different hexamer structures are consistent with 86 CVEs. As shown in figure 9, these

Table 1. Carbonyl saturation limits on nickel clusters and CVE counts

	$Ni_n(CO)_m^-$		$Ni_n(CO)_m$			$Ni_n(CO)_m^+$		Electron-counting rule predictions			
n	m^a	CVEs	m^b	m^c	CVEs[c]	m^d	CVEs	Structure[e]	CVEs	m (+, 0)	m(−)
3	6	43	8	9	48			Triangle	48	9	8
								Linear	50	10	9
4	9	59	10	10	60	10	59	Tetrahedron	60	10	9
								Butterfly	62	11	10
								Square	64	12	11
								Linear	66	13	12
5	12	75	11	11	72	12	73	Trigonal bipyramid	72	11	10
								Edge-bridged tetrahedron	74	12	11
								Square-pyramid	74	12	11
								Triangular array	76	13	12
								Bow-tie	78	14	13
								Pentagonal ring	80	15	14
								Linear	82	16	15
6	12	85	12	13	86	13	85	Bicapped tetrahedron	84	12	11
								Octahedron	86	13	12
								Capped square pyramid	86	13	12
								Edge-sharing tetrahedrons	86	13	12
								Edge-bridged trigonal bipyramid	86	13	12
								Pentagonal pyramid	88	14	13
								Trigonal prism	90	15	14
								Triangular arrays	90	15	14
								Hexagonal ring	96	18	17
								Linear	98	19	18
7	15	101	14	15	100	15	99	Capped octahedron	98	14	13
								Pentagonal pyramid	98	14	13
8	15	111	14	17	114	16	111	Bicapped octahedron	110	15	14
9	16	123	15	17	124	17	123	Tricapped octahedron	126	18	17
10	17	135	16	18	136	18	135	Tetracapped octahedron	140	20	19

[a] Maximum number of carbonyls adsorbed [135].
[b] Adsorption number for 'fast kinetics' [48].
[c] Adsorption number for saturation [48].
[d] Saturation limit [162].
[e] For $n > 6$, only the most compact structures (highest CVEs) are listed.

are an octahedron, a monocapped square pyramid, two tetrahedra sharing an edge, and a trigonal bipyramid with an extra edge-bridging metal atom. Thus, electron-counting rules become ambiguous for larger clusters. The electron-counting theories work well for rationalizing the geometric structures of organometallic complexes where the structure is already known by crystallography, but the inverse process of predicting a structure only by knowing the number of electrons may not give a unique answer, especially for larger clusters.

Table 1 shows observed saturation limits for CO on small nickel clusters. Nickel is one of the few systems for which CO saturation has now been measured for all three charge states of the clusters. We list values from our work for nickel cluster anions [115], from Parks *et al.* [48] for neutral nickel clusters and from Vajda *et al.* [162] for nickel cations. If the saturation limits strictly followed electron-counting rules and if the skeletal structures were the same for all three charge states, then the saturation limits would be the same for cationic and neutral clusters and that value minus one CO for anionic clusters. (The charged clusters have odd CVE counts, and we assume that a cluster with a singly occupied HOMO cannot accept two more electrons to bind an additional CO molecule.) This behaviour is in fact observed for $n = 4$, 6, 9 and 10, but not for $n = 3$, 5, 7 and 8, that is in just half the cases that can be compared. That does not necessarily mean a failure of the electron-counting rules, because the different charge states could possess different skeletal structures in some cases. On the other hand, Parks *et al.* [48] found that their saturation limits can reasonably be attributed to packing limits using van der Waals radii for the carbonyls and the bulk Ni—Ni bond distances for the clusters. They also proposed that the structures may undergo rearrangements as COs are added [48]. The propensities for isomerization depend both on the available energy from binding an additional CO and on the rate at which that energy is removed by stabilizing collisions. The latter in turn depends on the kinetic conditions (buffer gas density, CO density and reaction time), which are quite different for the three experiments. Ideally, theoretical calculations might be able to determine the most stable structures for the saturated nickel cluster carbonyl in the three charge states. However, electronic structure calculations are still quite challenging for transition-metal clusters of this size, and saturation limits alone do not provide a particularly stringent test for comparing experiments with theory.

4. Metal–carbonyl dissociation energies

While chemisorption saturation limits in conjunction with electron-counting rules or other structural models provide clues about the skeletal structures of the clusters, it is desirable to obtain site-specific information about the ligands. Specifically, we want to know the geometry of the binding sites of the carbonyls and the electronic character of the metal—ligand bonding. The metal—ligand dissociation energy is a key property in this regard. Adsorbate binding energies have been related to structural features of metal clusters [170–173]. We have used threshold collision-induced dissociation (TCID) experiments to measure binding energies of CO adsorbed on small copper, platinum and palladium cluster anions [124, 138, 174, 175].

4.1. *Guided-ion-beam mass spectrometry studies*

The experiments are carried out in our guided-ion-beam tandem mass spectrometer [176], shown in figure 10. The metal cluster ion source is an ion flow tube reactor as described above. Negative cluster ions are extracted through a small aperture (1–2 mm

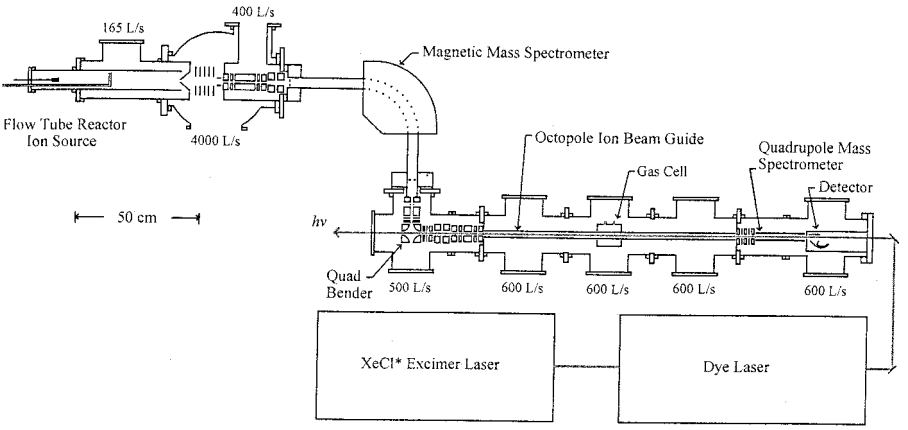

Figure 10. Schematic diagram of the guided-ion beam tandem mass spectrometer and laser system.

diameter) in a nose cone at the end of the flow tube, are focused and accelerated, and are then selected by mass using a magnetic sector. The initial mass selection of reactant cluster ions is a major advantage over the ion flow tube reactor experiments described above. The cluster anions are then decelerated and injected into a rf octopole ion-beam guide (1 m long) at a controlled translational energy. The ion-beam guide creates a effective radial ion-trapping field without significantly affecting the axial ion energies [177]. At its midpoint, the octopole passes through a gas collision cell where the reactant or target gas is introduced. Reactant and product ions are collected with high efficiency by the octopole trap and then mass analysed by a quadrupole mass spectrometer. Ions are detected by a collision dynode and particle multiplier using pulse counting. Reaction cross-sections are obtained from the ratios of reactant and product ion intensities as a function of collision energy [176, 178]. Effective cross-sections are obtained at several reactant gas pressures (0.03–0.30 mTorr) and extrapolated to zero pressure to obtain the cross-sections in the single-collision limit.

Laboratory ion energies are measured by both retarding potential analysis and time-of-flight measurements [176] and converted to centre-of-mass frame collision energies [178]. For the time-of-flight measurements, the ion beam is pulsed by a set of deflectors preceding the octopole. The measured ion-beam energy spread is typically 0.15–0.30 eV. Further details of our guided-ion-beam tandem mass spectrometer and data analysis have been presented previously [25, 176].

Meticulous but routine data analysis procedures are required to obtain accurate threshold energies from the experimentally broadened TCID data, as described elsewhere [176, 178–181]. We fit the data with an empirical threshold law with the basic form of

$$\sigma(E) = \sigma_0 \frac{(E - E_0)^N}{E}, \tag{5}$$

where $\sigma(E)$ is the cross-section as a function of collision energy, E_0 is the threshold energy, and σ_0 and N are adjustable parameters. This widely used form has been justified elsewhere [23, 176, 181, 182]. We use the CRUNCH program [183] to include convolutions over translational energy distributions and the thermal internal energy

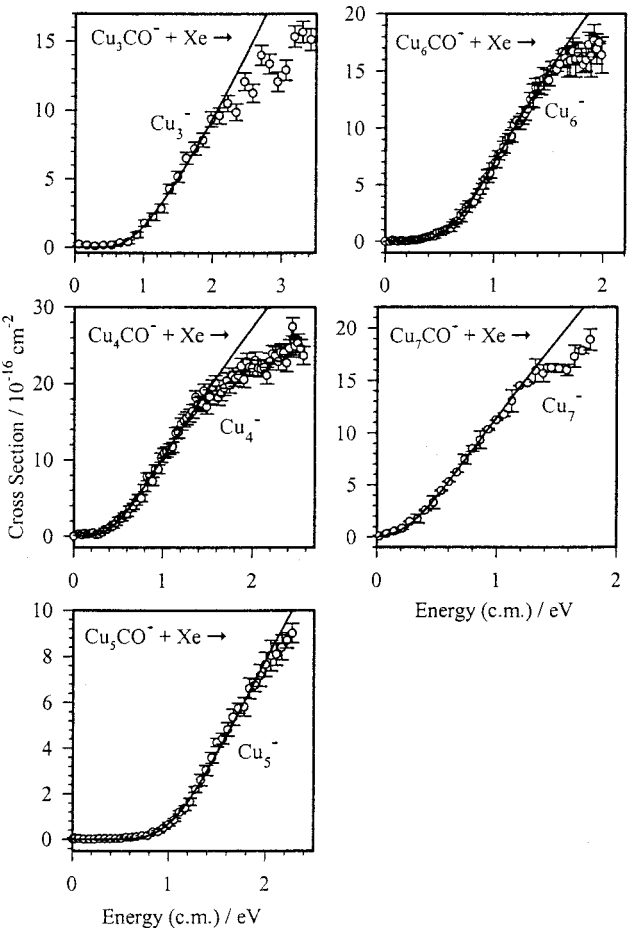

Figure 11. Cross-section for collision-induced dissociation of CO from Cu_nCO^- (n = 3–7) as a function of collision energy in the centre-of-mass frame with the xenon target gas: (——), fits of the threshold model including convolutions over the experimental energy distributions and the detection probability, taking into account kinetic shifts.

of the reactants [103, 178, 184]. For TCID, we also correct for kinetic and competitive shifts using Rice–Ramperger–Kassel–Marcus (RRKM) theory [123, 179, 180]. Details of these procedures have been described thoroughly in recent articles [123, 179–181]. When applied with care, TCID measurements provide accurate reaction threshold energies within the conservatively stated uncertainty limits.

4.2. *Threshold collision-induced dissociation*

Energy-resolved TCID is used to measure both metal–metal binding energies for bare metal clusters and the binding energies of adsorbates on clusters [25, 124, 125, 138, 174, 175]. Recent examples of TCID data and the threshold model fits [124], for loss of CO from Cu_nCO^- (n = 3–7), are shown in figure 11.

Strictly, the TCID threshold energy is an upper limit to the thermodynamic endoergicity (bond dissociation energy). The threshold energy represents the true thermochemical threshold, $E_0 = \Delta_r H_0$, in the absence of a barrier in excess of the

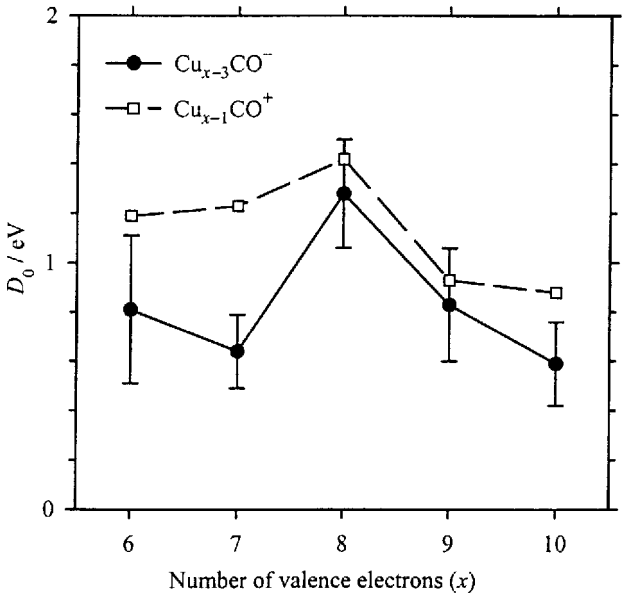

Figure 12. Dissociation energies for loss of CO from copper cluster monocarbonyls as a function of the number x of CVEs: (●), experimental threshold energies from TCID experiments [124] on the anionic species, $Cu_{x-3}CO^-$; (□), theoretical dissociation energies [199] for the cationic species, $Cu_{x-1}CO^+$.

reaction endothermicity (i.e. no reverse activation energy) or a dynamic restriction to reaction at threshold. Reaction threshold energies at the thermochemical endothermicity are typical for collision-induced dissociation of ionic clusters because the barriers that might exist for comparable neutral systems are eliminated by the strong ion–induced-dipole attractive potential [23, 182]. Many systems for which independent thermochemical values are available show thresholds at the thermodynamic limit [23, 103, 179, 185–187]. There are of course examples of endoergic and exoergic ion–molecule reactions with excess barriers, for reactions that are spin forbidden, that require non-adiabatic transitions between electronic surfaces or that have dynamical constraints for passage through a tight transition state [176, 188–192]. For the collision-induced dissociation of transition-metal clusters, we expect there to be no reverse activation barriers because the large number of low-lying electronic states are efficiently coupled to the ground-state dissociation asymptote through spin–orbit and vibronic coupling. Photodissociation experiments on transition-metal dimers and trimers show prompt dissociation at the asymptotic limit [193–197]. For heterolytic dissociation processes, as in the removal of a CO ligand that takes with it both electrons of the σ bond, molecular orbital arguments indicate there should be no barrier [143], and this is corroborated by our observation of rapid rates for the reverse CO addition to the cluster ions under room-temperature thermal conditions [135, 174].

Carbonyls adsorb to the copper-group clusters by donation of the two electrons from the CO lone-pair orbital into the delocalized cluster lowest unoccupied molecular orbital (LUMO) [115, 198]. The CO binding energies for the copper cluster anions [124] obtained from the TCID threshold fits in figure 11 are shown in figure 12, together with theoretical values for cationic clusters [199]. These are both plotted as a function of the number of cluster valence electrons, including the two electrons

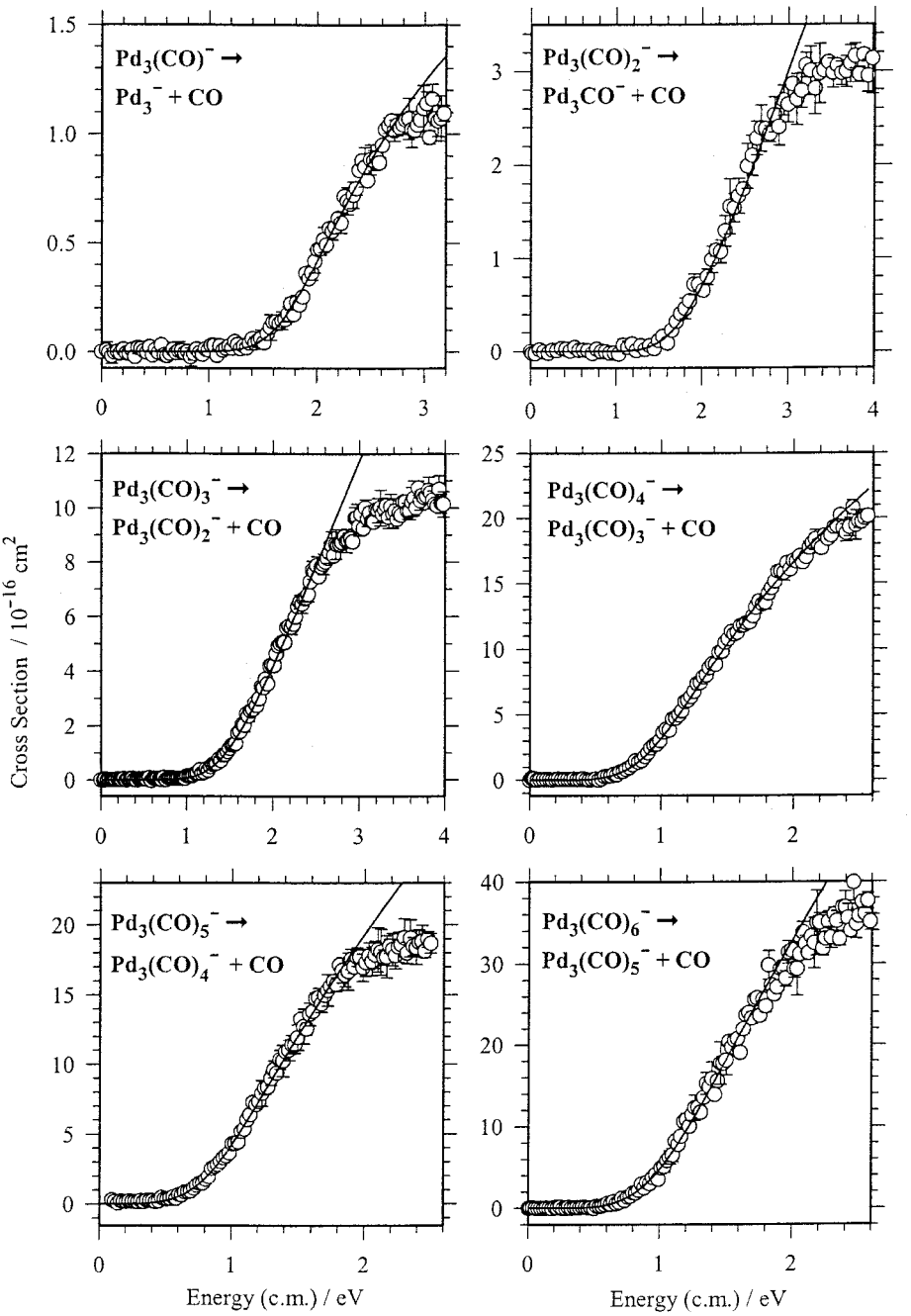

Figure 13. Cross-section for collision-induced dissociation of CO from $Pd_3(CO)_m^-$ (m = 1–6) as a function of collision energy in the centre-of-mass (c.m.) frame with the xenon target gas: (——), fits of the threshold model including convolutions over the experimental energy distributions and the detection probability, taking into account kinetic shifts.

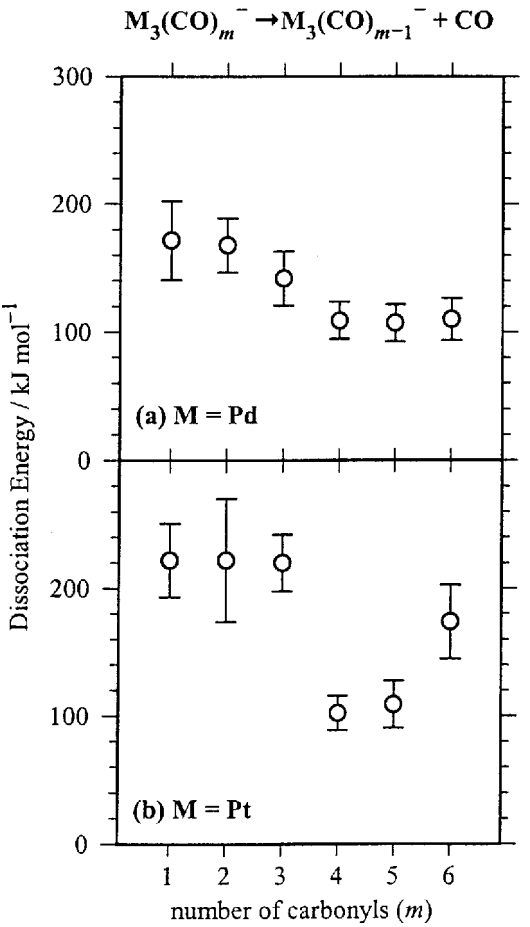

Figure 14. Dissociation energies for the loss of CO from $M_3(CO)_m^-$ (M = Pd or Pt; m = 1–6) as a function the initial number m of adsorbed CO molecules from TCID measurements.

donated by the CO. The eight-electron species Cu_5CO^- and Cu_7CO^+ show higher stability than their neighbours because they have a closed shell of eight cluster valence electrons in the jellium model [124]. This is an instance where the carbonyl ligand interacts with a delocalized cluster orbital, rather than a localized binding site at a metal centre. The σ donor orbital interacts primarily with the delocalized LUMO, π back bonding is probably not important because the filled d-shell orbitals are low in energy and localized on the copper atoms, and the geometry of the carbonyl binding site is not a critical factor.

In contrast with the copper clusters, the binding energies of multiple carbonyls on open d-shell metals show differences that can be attributed to specific binding sites. We have measured TCID threshold energies for removal of CO from palladium and platinum trimer anions, $M_3(CO)_m^-$ (m = 1–6), as well as some larger platinum clusters with either one carbonyl or saturated with carbonyls [114, 138, 174]. The TCID data for $Pd_3(CO)_m^-$ (m = 1–6) are shown in figure 13 and the dissociation threshold energies for palladium and platinum trimer anions are shown in figure 14 [114, 138, 174]. The threshold energies represent the energy to remove one carbonyl from trimer clusters initially with one to six carbonyls adsorbed. These represent measurements of *site-*

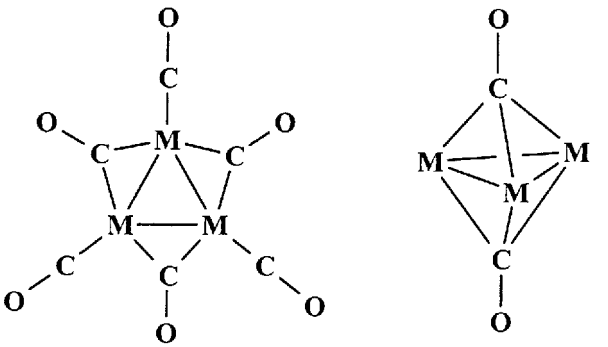

I **II**

Figure 15. Proposed structures of palladium or platinum trimer carbonyls.

specific individual binding energies of ligands on multimetal clusters. Calorimetric studies [82] provide only average binding energies for ligands of different types and rely on assignment of the relative values for metal–carbonyl versus metal–metal dissociation energies.

The saturated platinum trimer anion $Pt_3(CO)_6^-$ has the same stoichiometry as a known condensed-phase species [200], $[Pt_3(CO)_3(\mu\text{-}CO)_3]^{2-}$, which has a quasiplanar structure with three terminal carbonyls and three edge-bridging carbonyls (structure **I** in figure 15). It would seem reasonable that the saturated gas-phase species $M_3(CO)_6^-$ (M = Ni, Pd or Pt) also have this structure, but the saturation limits alone do not provide sufficient information for a definitive assignment. The sequential carbonyl binding energies provide further clues. For platinum (figure 14(*b*)), the first three carbonyls have high threshold energies of around 220 kJ mol^{-1}, followed by a sharp drop to about 100–110 kJ mol^{-1} for the fourth and fifth carbonyls and then an intermediate value for removing a carbonyl from the saturated species with six carbonyls. The large variation in binding energies implies that the ligands are not fluxional, that is they have preferred binding sites. We interpret [138, 174] the sharp drop in binding energy between the third and fourth carbonyls in $Pt_3(CO)_m^-$ as indicating two different binding sites, consistent with structure **I**. The first three carbonyls add to stronger-binding bridging sites and the second three carbonyls add to terminal sites. We assign the stronger-binding sites to bridged carbonyls primarily on the basis of the known infrared spectra of the CO moiety. In the condensed-phase compounds, bridged carbonyls have lower CO stretching frequencies than do terminal carbonyls, which indicates stronger π back bonding and therefore stronger metal—carbon bonding for the bridged species [200–202]. Early extended Hückel molecular orbital calculations on triplatinum compounds also suggest that bridging carbonyls are more strongly bound than terminal carbonyls [203, 204]. High-level calculations including relativistic effects on Pt_2CO neutral by Rozak and Balasubramanian [205] indicate that the bridged tee-shaped species is 95 kJ mol^{-1} more stable than the linear terminally bound species, consistent with the relative dissociation energies for $Pt_3(CO)_m^-$ in figure 14(*b*). Density functional theory calculations [206] that have appeared recently for neutral Pt_3CO agree well with our Pt_3^-–CO binding energy of about 220 kJ mol^{-1} but indicate that the bridging and terminal binding sites are about equally favourable for one CO on Pt_3. If that result holds for the anion, then the simple picture of sequential addition first to the three bridging sites followed by

addition to the three terminal sites would need to be revised. It is plausible that the carbonyls are fluxional on the highly unsaturated species formed initially but then become fixed once the three more favourable bridging positions become filled. However, to be really convincing a theoretical calculation, firstly, should be made on the anionic species actually studied and, secondly, should predict the experimental binding energy trend for all six species (m = 1–6) in figure 14(*b*). As electronic structure calculations for transition-metal clusters improve, theory will become increasingly important for relating geometries to the measured metal–ligand dissociation energies.

The intermediate binding energy of the sixth carbonyl on triplatinum anion, higher than the terminal carbonyls for the fourth and fifth positions (figure 14(*b*)), may reasonably be attributed to extra electronic stability of the near-closed-shell saturated $Pt_3(CO)_6^-$ species. The negative-ion photoelectron spectrum [207, 208] of $Pt_3(CO)_6^-$ shows a large HOMO–LUMO band gap, which is not present for $Pt_3(CO)_m^-$ for $m <$ 6.

For larger $Pt_n(CO)_m^-$ (n = 4–6) species, we use the characteristic binding energies for terminal and bridging carbonyls from $Pt_3(CO)_m^-$ to assign the terminal and bridging carbonyl geometries [174]. In each case, the first carbonyl that adds to one of the larger clusters is strongly bound, consistent with a bridging site. For the platinum clusters that are fully saturated with CO, removing one carbonyl takes 100 kJ mol^{-1} or less, consistent with more weakly bound terminal carbonyls. It is also possible that the CO binding energy for the saturated species is further weakened by steric crowding, as suggested by the work of Parks *et al.* [47, 48] on CO saturation of neutral nickel clusters.

We also performed TCID experiments on the bare platinum cluster anions [174]. The threshold energies for loss of a platinum atom from platinum clusters are higher, greater than 400 kJ mol^{-1}. This explains why only loss of carbonyl is seen in TCID for most of the platinum cluster carbonyl ions. The only exception is $Pt_3(CO)_2^-$, for which another product channel competes with loss of carbonyl, namely formation of $Pt_2CO + PtCO$. The neutral PtCO species is evidently quite stable thermochemically. Because of the uncertainty in treating the two-channel process, the TCID threshold energy for $Pt_3(CO)_2^-$ in figure 14(*b*) has a larger error bar than for the other processes. We shall re-examine this system in the time-resolved photodissociation (TRPD) experiments discussed in section 5.

As shown in figure 14, the palladium trimer anion carbonyls show a different trend in the sequential binding energies compared with the platinum trimer [137, 174, 175]. The stepwise drop in binding energies of $Pd_3(CO)_n^-$ from n = 2 to n = 4 (rather than the sharp drop after n = 3 for the platinum system) is consistent with formation of a symmetric bipyramidal $Pd_3(CO)_2^-$ intermediate with the carbonyls on the two face sites (structure **II** in figure 15) [175]. After these first two carbonyls, additional carbonyls would fill the edge or terminal sites, possibly with rearrangement to structure **I** by the time that the saturation limit is reached at $Pd_3(CO)_6^-$. The negative-ion photoelectron spectrum of $Pd_3(CO)_2^-$ shows sharp features corresponding to a large HOMO–LUMO bandgap, which is not present for $Pt_3(CO)_2$ and which suggests $Pd_3(CO)_2$ may be an electronically stable symmetric species [207, 208]. Further supporting evidence for structure **II** includes the propensity for CO to bind at threefold sites on palladium surfaces, whereas threefold binding sites are absent on platinum surfaces [209, 210]. Limited theoretical information is available for palladium carbonyls [211, 212]; further theoretical examination would be helpful to test our structural inferences from

the binding energies. Our measured binding energies, especially the trends for sequential addition of carbonyls to the clusters, provide important experimental benchmarks to gauge the quality of theoretical calculations.

5. Time-resolved photodissociation

As an alternative to collision-induced dissociation, we have conducted TRPD lifetime experiments to determine binding energies of transition-metal cluster anions and adsorbates on the clusters [114, 123, 125]. Photodissociation measurements have also been employed to obtain binding energies of cationic metal clusters [22, 122, 196, 213–219] and other transition-metal-containing ions [220, 221]. In the TRPD technique [22, 122, 123, 222, 223], the rate of unimolecular dissociation is measured directly by monitoring the ion fragmentation probability as a function of time following photoactivation. TRPD is an attractive alternative to collision-induced dissociation because the amount of energy deposited is exactly equal to the photon energy and is not a distribution due to random impact parameters as in TCID. The fragmentation dissociation probability as a function of time is modelled using the RRKM theory of statistical unimolecular decomposition to extract the binding energy.

For our cluster ion TRPD measurements, the output of a dye laser pumped by a 400 Hz XeCl excimer laser (Lambda Physik) is passed coaxially with the ion beam through the octopole region as shown in figure 10. The laser dissociation experiment is illustrated in figure 16. In a continuous beam, the mass-selected ions pass at constant velocity through the octopole towards the detector. The laser pulse (20 ns) excites at once the entire volume of the ion beam along the octopole axis. Ions are counted as they arrive at the detector as a function of time from the laser pulse using a multichannel scaler. Ions located near the end of the octopole when the laser fires have less time to fragment than ions located at the beginning of the octopole. In effect, the spatial distribution of ions in the octopole is converted into a time distribution. With the quadrupole mass spectrometer turned to the fragmentation product ion mass, we obtain a time spectrum showing the rise time of fragment ions, which provides a direct measurement of the unimolecular dissociation rate.

Platinum carbonyl cluster anions are readily dissociated by visible photons, leading primarily to loss of CO ligands. The clusters adsorb and dissociate over broad wavelength ranges, as expected by their high density of electronic states, but they show slow statistical decomposition lifetimes only over restricted regions. We were able to obtain TRPD spectra for $Pt_3(CO)_m^-$ (m = 2, 3, 6). Figure 17 shows a set of TRPD spectra for $Pt_3(CO)_3^-$ at various wavelengths. The fragmentation product ion intensities are plotted as a function of the time after the laser pulse. The photofragment rise times are faster for higher photon energies (lower wavelength) than for lower photon energies, as expected for a statistical decomposition process.

To fit the time-resolved photodissociation data, we use [123]

$$I(t) = C\int_0^\infty\int_0^\infty P(E_{\mathrm{vib}}, J)\{1-\exp[-k_{\mathrm{RRKM}}(E, J)(t-t_0)]\}\,\mathrm{d}J\,\mathrm{d}E_{\mathrm{vib}}, \tag{6}$$

where $I(t)$ is the observed fragment ion intensity versus time t from the laser pulse, t_0 is the instrumental delay time (time-of-flight of ions from the end of the octopole to the detector), C is a scaling constant and $P(E_{\mathrm{vib}}, J)$ is the thermal Boltzmann distribution

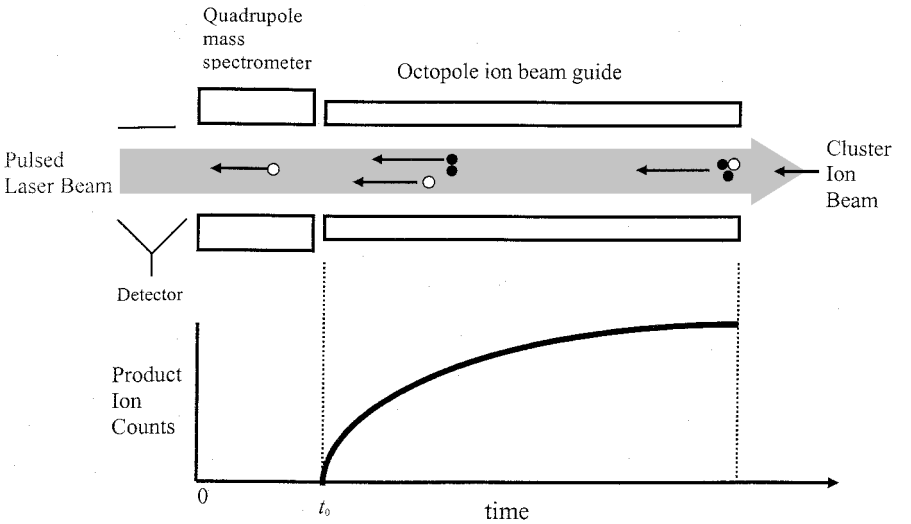

Figure 16. Schematic diagram illustrating the TRPD.

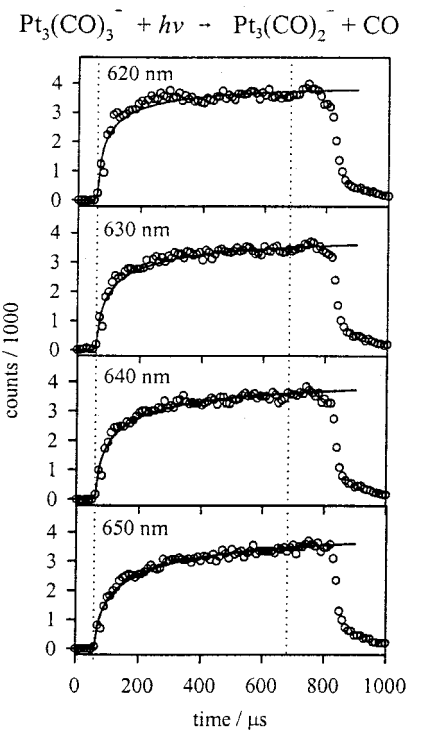

Figure 17. TRPD of $Pt_3(CO)_3^-$ for four laser wavelengths: (○), intensities of the $Pt_3(CO)_2^-$ photofragment ions as a function of time from the laser pulse; (· · · ·), vertical lines enclosing the ions that are positioned in the octopole at the time of the laser pulse; (——), RRKM fits of the dissociation probabilities.

of the cluster ion vibrational energies E_{vib} and rotational states J at the source temperature of 300 K. The microcanonical RRKM dissociation rate k_{RRKM} is given by [224, 225]

$$k_{RRKM}(E, J) = s\frac{W^{\ddagger}(E-E_0, J)}{h\rho(E, J)}, \tag{7}$$

where $E = E_{vib}+E_{rot}+E_{h\nu}$ is the total available energy, $E_{h\nu}$ is the photon energy, E_0 is the binding energy, $W^{\ddagger}$ is the sum of states at the transition state, ρ is the density of states of the cluster and s is the reaction degeneracy. The implementation of RRKM theory is the same as described for our TCID work [179, 180, 226]. We can be assured that the fragmentation processes are statistical in nature because of the time frame of the experiments. The experimental time window ranges from about 10 μs to 1 ms (variable by changing the ion-beam energy in the octopole region), a sufficient time for randomization of internal degrees of freedom. The RRKM rate is extremely sensitive to the binding energy E_0 but relatively insensitive to cluster vibrational and rotational constants, which we estimate using simple models [114, 123, 125, 174, 175, 227]. For loss of CO, which is a barrierless process as discussed above, a loose 'orbiting' transition state model is used [179]. The transition state is vibrationally located at the top of the centrifugal barrier of the ion–induced-dipole potential, with vibrations and rotations equal to those of the products.

Fragmentation might compete with electron loss or radiative stabilization from a common statistically excited $[M_nL^-]^*$ intermediate:

$$\begin{aligned} M_nL^- + h\nu \rightarrow [M_nL^-]^* &\rightarrow M_n^- + L \qquad k_1 \\ &\rightarrow M_nL + e^- \qquad k_2 \\ &\rightarrow M_nL^- + h\nu' \qquad k_3 \end{aligned}$$

The integrated rate law for the observed fragment ion channel is

$$[M_n^-]_t = I(t) = [M_nL^-]_0\frac{k_1}{k_{tot}}[1-\exp(-k_{tot}\,t)],$$

which indicates that the rate that we measure from the product time profile is actually the total rate $k_{tot} = k_1+k_2+k_3$. Therefore, to compare the dissociation rate k_1 with statistical theory, the branching ratios should be determined. We cannot detect electrons or photons directly. However, electron loss can be detected indirectly by comparing the total photodepletion of reactions ions M_nL^- with the intensity of products M_n^-. This allows us to determine the branching ratio between k_1 and k_2. Unfortunately, the experiment is completely blind to radiative stabilization of the photoactivated cluster ion.

For TRPD of bare silver and gold cluster anions [123, 125], we measured branching fractions for dissociation and electron emission. Comparison of the derived dissociation energies with TCID experiments on the same ions show general agreement, within the mutual error bars for most sizes. However, the TCID values are systematically higher than the TRPD values by a small amount for Ag_n^- (n = 7–11) and Au_n^- (n = 6, 7). This systematic deviation might be attributed to, firstly, the slightly less efficient energy transfer upon collision than is predicted by the threshold model in equation (5), secondly, the influence of electron loss for TCID in competition with fragmentation or, thirdly, the influence of radiative stabilization in either TCID or TRPD. Estimation of the radiative emission rates for gold clusters [125] implies that radiative emission is too slow to affect the experiments, given the

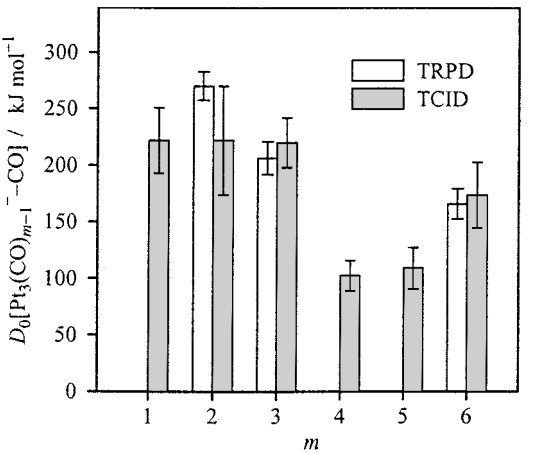

Figure 18. Comparison of results from TCID and TRPD for the dissociation energies for loss of CO from $Pt_3(CO)_m^-$ ions.

instrumental time windows. Based upon these results, we expect TCID and TRPD to give similar results, with the dissociation energies from TRPD to be slightly lower and probably more accurate.

For removal of adsorbates such as CO, the desorption energy is usually less than the photodetachment energy. This is the case for $Pt_3(CO)_m^-$ species [114, 207, 208], and our TRPD measurements of the total ion depletion confirm that there is no electron loss in competition with CO loss. The presence of the carbonyl ligand may increase radiative emission rates because of its oscillator strength, but it is unknown by how much. Therefore, we are forced to neglect radiative emission as a competitive process. Figure 18 compares the carbonyl dissociation energies from TRPD for $Pt_3(CO)_m^-$ (m = 2, 3, 6) [114] with our earlier values from TCID [138, 174]. The values agree within their experimental uncertainties for all three species. For m = 3 and 6, the TCID values are slightly higher as expected from our experience with silver and gold cluster anions. For $Pt_3(CO)_2^-$, however, the TRPD dissociation energy is higher than the TCID value, at the upper end of the error bar of the latter. As noted in section 4, $Pt_3(CO)_m^-$ was unique among these systems in that a competition between two fragmentation channels was observed, formation of PtCO neutral in addition to simple CO loss. Curiously, photodissociation yields only CO loss. Further investigation [114] using TCID showed that at least two isomers are present in the $Pt_3(CO)_2^-$ cluster beam. The relative isomer intensities can be changed by using extreme conditions in the ion flow tube reactor (reducing the helium buffer gas pressure by a factor of four). The lack of PtCO loss in TRPD can be explained only if, firstly, one of the isomers does not adsorb at the laser wavelength used or, secondly, the dissociation is highly non-statistical. Unfortunately, the available experimental information does not allow us to make any definitive conclusions about the possible structures of the $Pt_3(CO)_2^-$. Theoretical calculations would be useful in this regard. As a general comment, these studies show the utility of applying more than one experimental technique to an experimental problem.

6. Gas-phase metal cluster catalysis

Gas-phase metal clusters are excellent models for catalytic processes, with the capability of microscopic control of the size and energies of the metal particles. However, the use of gas-phase metal clusters as actual catalysts has been extremely

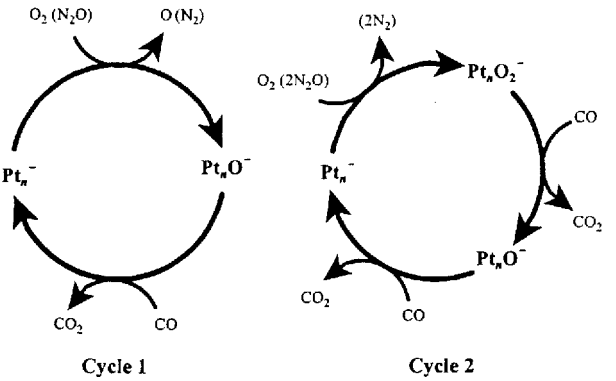

Figure 19. Catalytic cycles observed for the oxidation of CO to CO_2 by N_2O or O_2 using gas-phase platinum cluster anions as the catalyst.

limited. Irion and co-workers [5] used ion cyclotron resonance experiments to demonstrate the use of iron cluster cations for the 'catalytic' conversion of ethylene to benzene, but the removal of benzene in the final step to regenerate the initial iron cluster required addition of at least 3.2 eV in a collision-induced dissociation step. Catalytic processes promoted by *atomic* gas-phase transition-metal cations have also been observed [228–232].

We recently demonstrated that gas-phase platinum cluster anions, Pt_n^- (n = 3–7), efficiently catalyse the oxidation of CO to CO_2 by N_2O or O_2 near room temperature as illustrated by the cycles in figure 19 [6]. This is the first report of a transition-metal cluster catalyst that undergoes a full thermal catalytic reaction cycle, defined as a process in which the intact cluster is regenerated at the end and each step is exothermic and occurs rapidly at thermal energies. Experimental mass spectra are shown in figure 20 for the example of Pt_4^-. The dc discharge metal cluster source produces Pt_4^- clusters in the flow tube and thermalized by collisions with the buffer gas. When either O_2 or N_2O is introduced at a downstream point in the flow tube, Pt_nO^- and $Pt_nO_2^-$ ions are formed in rapid exothermic reactions as measured previously [137]. Figure 20 is a mass scan of the quadrupole mass spectrometer showing the regeneration of Pt_4^- when CO is introduced to the gas cell. The only possible neutral product at low energies is CO_2, and there is negligible fragmentation of the metal cluster for $n \geqslant 4$. Cross-section measurements as a function of translational energy for this catalytic oxidation of CO are shown in figure 21. At low energies, the cross-section approaches the calculated collision limit, that is the reactions are quite efficient. When $Pt_nO_2^-$ ions are selected initially, we observe sequential loss of oxygen atoms to form two CO_2 products, as shown by CO pressure dependence studies. This observation implies that O_2 is dissociatively adsorbed on the metal cluster as oxygen atoms, rather than chemisorbed or physisorbed as molecular O_2. Two other observations support this conclusion.

(1) $Pt_nO_2^-$ ions produced by reaction of the bare cluster with either O_2 or N_2O show the same reactivity,
(2) Collision-induced dissociation of $Pt_nO_2^-$ shows loss of oxygen atoms with no O_2 loss.

The regeneration of Pt_n^- ions at low energies proves that a full catalytic oxidation cycle can be completed at near room temperature, in either a single-step or a two-step

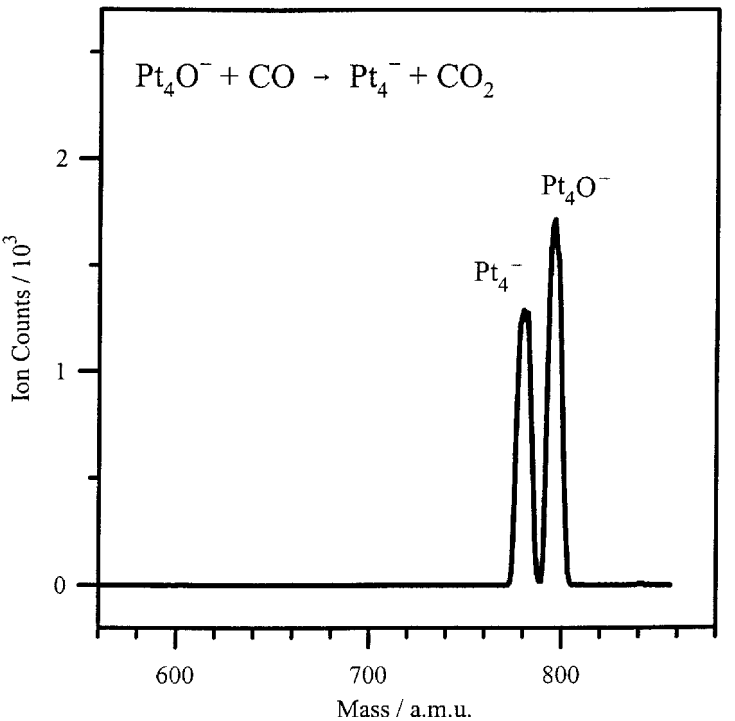

Figure 20. Mass spectra for the reaction $Pt_4O^- + CO \rightarrow Pt_4^- + CO_2$ at centre-of-mass energy of 0.05 eV and a gas cell pressure of 0.2 mTorr. The Pt_4O^- is isolated by mass prior to reaction with CO in the gas cell of the octopole ion beam guide. Isotopic peaks are not resolved at the quadrupole mass resolution used. Under these conditions, the catalytic conversion to CO_2 has occurred for about 40% of the ions.

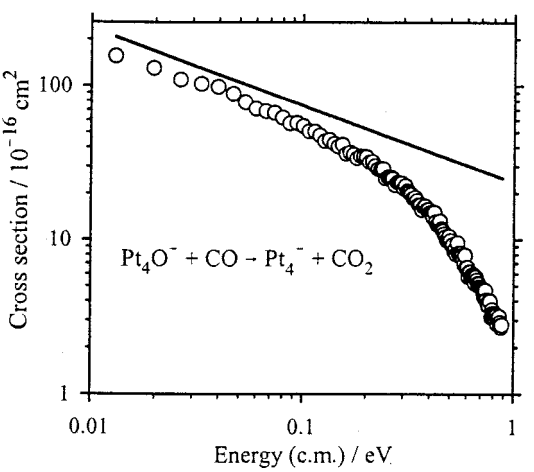

Figure 21. Cross-sections (○) for the reaction $Pt_4O^- + CO \rightarrow Pt_4^- + CO_2$ as a function of collision energy in the centre-of-mass (c.m.) frame: (——), calculated collision cross-section.

process as shown in figure 19. The recovered platinum ion could in principle initiate a new cycle, although they are of course destroyed by being detected in our experiment. Figure 22 shows the measured reaction efficiencies for the oxidation of the first CO molecule by Pt_nO^- or $Pt_nO_2^-$ (n = 3–6). The reaction efficiencies for a single collision

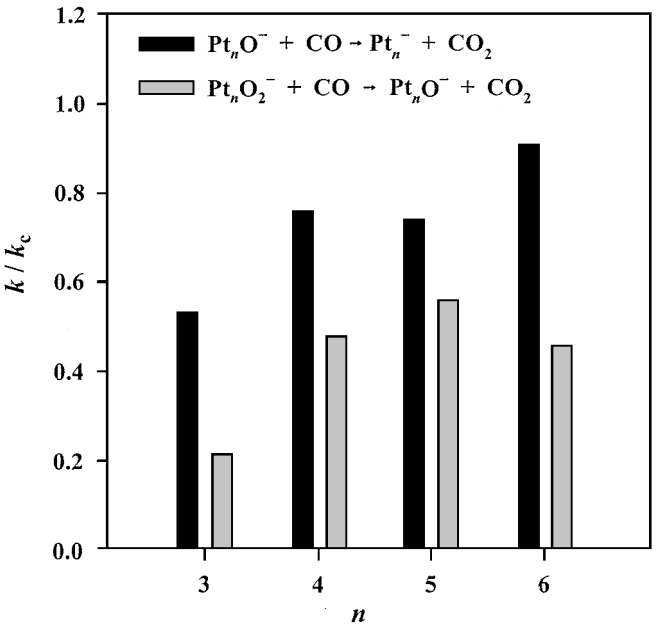

Figure 22. Relative reaction efficiencies for the conversion of CO to CO_2 by $Pt_nO_m^-$ clusters of various compositions.

are greater than 40% for $n \geqslant 4$; so only a few collisions would be required for complete conversion. The observation of these efficient catalytic reactions at near room temperatures implies that the gas-phase metal cluster anions are better catalysts than the supported catalysts used in current technology for automotive catalytic converters, which need to be heated to high temperatures [83]. On platinum surfaces, temperatures of 400–500 K are typically required for oxidation of CO [233–236]. The high reactivity of the clusters may be attributable to their small size, which means that the metal atoms are all exposed on the surface of the clusters and are coordinatively highly unsaturated. In addition, the negative charge of our cluster anions may be important. Excess electron density promotes CO_2 dissociation on doped platinum surfaces [237]; so the negative charge might also lower the energy of the transition state for oxidation.

It is an interesting exercise to consider the possible practical use of gas-phase metal cluster catalysis. One could, in principle, design an ion trap reactor in which the metal cluster ions are held and through which CO and O_2 reactants flow. In that case, a relevant question is whether the reaction can occur in a different order from that observed, that is with initial chemisorption of CO to form Pt_nCO^- followed by reaction with O_2. Our examination of the latter reaction in the collision cell of the guided-ion-beam apparatus [6] shows that extensive fragmentation of the cluster occurs owing to the high exothermicity of the reaction. Similarly, reaction of the bare platinum cluster anions with O_2 in the collision cell results in extensive fragmentation, that is destruction of the catalyst. The reason that the oxidation step proceeds with much less fragmentation in the flow tube reactor source is that collisions with buffer gas carry away the excess energy before the clusters dissociate. This points to a fundamental difference between gas-phase cluster catalysis and either homogeneous catalysis in solution or heterogeneous catalysis on surfaces. In those cases, the solvent

or bulk metal naturally provides a heat bath that removes the excess energy from the exothermic overall reaction. For gas-phase cluster catalysis to work in a practical reactor, the buffer gas density would have to be optimized such that there are enough collisions to stabilize the regenerated metal clusters before they dissociate, but not so many that the chemisorbed reaction intermediates or products are completely stabilized on the surface of the clusters.

In work in progress, we are examining the use of palladium cluster anions for the analogous catalytic oxidation of CO to CO_2 [238]. The palladium clusters also efficiently catalyse the oxidation reaction. The palladium clusters show more cluster fragmentation than the platinum clusters, consistent with the weaker metal—metal bond strengths in palladium relative to platinum.

7. Conclusions

The experiments discussed here demonstrate how metal–ligand interactions can be used to probe the electronic and geometric structure of transition-metal clusters. Mass spectrometry and laser photodissociation experiments are well suited to these studies because of their ability to study a single size-selected cluster species. A full understanding of the reactivity of metal clusters, for example their catalytic activity, will require more detailed knowledge about the metal–ligand interactions for intermediates along the reaction pathways. The rapid advancement of theoretical methods for transition-metal species will allow a better correlation between the physical and chemical properties of the clusters and their structural features.

Acknowledgements

I am grateful to the students and post-doctoral research associates who have been involved in aspects of this research: Xiaoli Ren, Paul A. Hintz, Elizabeth Kapiloff, Taeck-Hong Lee, Alexandre A. Shvartsburg, Joseph Mwakapumba, Alexander Grushow, John P. Maberry, Vincent F. DeTuri, Vassi A. Spasov, Yang Shi and Moses Dogbevia. Our transition-metal cluster research has been supported by the National Science Foundation and the University of Nevada, Reno. The donors of the Petroleum Research Fund, administered by the American Chemical Society, are acknowledged for partial support of this research.

References

[1] Doesburg, E. B. M., and van Hooff, J. H. C., 1993, *Catalysis. An Integrated Approach to Homogeneous, Heterogeneous and Industrial Catalysis*, edited by J. A. Moulijn, P. W. N. M. van Leeuwen and R. A. van Santen (Amsterdam: Elsevier), p. 309.
[2] Gates, B. C., 1995, *Chem. Rev.*, **95**, 511.
[3] Heiz, U., Sanchez S., Albert, S., and Schneider, W.-D., 1999, *J. Am. chem. Soc.*, **121**, 3214.
[4] Sanchez, A., Abbet, S., Heiz, U., Schneider, W.-D., Häkkinen, H., Barnett, R. N., and Landman, U., 1999, *J. phys. Chem.* A, **103**, 9573.
[5] Schnabel, P., Weil, K. G., and Irion, M. P., 1992, *Angew. Chem., Int. Edn Engl.*, **31**, 636.
[6] Shi, Y., and Ervin, K. M., 1998, *J. chem. Phys.*, **108**, 1757.
[7] Dietz, T. G., Duncan, M. A., Powers, D. E., and Smalley, R. E., 1981, *J. chem. Phys.*, **74**, 6511.
[8] Riley, S. J., Parks, E. K., Mao, C.-R., Pobo, L. G., and Wexler, S., 1982, *J. phys. Chem.*, **86**, 3911.
[9] Geusic, M. E., Morse, M. D., and Smalley, R. E., 1985, *J. chem. Phys.*, **82**, 590.

[10] TREVOR, D. J., WHETTEN, R. L., COX, D. M., and KALDOR, A., 1985, *J. Am. chem. Soc.*, **1985**, 518.
[11] ZAKIN, M. R., BRICKMAN, R. O., COX, D. M., and KALDOR, A., 1988, *J. chem. Phys.*, **88**, 5943.
[12] SMALLEY, R. E., 1985, *Comparison of Ab Initio Quantum Chemistry with Experiment for Small Molecules*, edited by R. J. J. Bartlett (Dordrecht: Reidel), p. 53.
[13] RILEY, S. J., 1994, *Clusters of Atoms and Molecules II*, edited by H. Haberland (Berlin: Springer), p. 221.
[14] PARKS, E. K., KLOTS, T. D., and RILEY, S. J., 1990, *J. chem. Phys.*, **92**, 3813.
[15] KORETSKY, G. M., and KNICKELBEIN, M. B., 1997, *J. chem. Phys.*, **106**, 9810.
[16] ERVIN, K. M., and LINEBERGER, W. C., 1992, *Advances in Gas Phase Ion Chemistry*, Vol. 1, edited by N. G. Adams and L. M. Babcock (Greenwich, Connecticut: JAI), p. 121.
[17] YOSHIDA, H., TERASAKI, A., KOBAYASHI, K., TSUKADA, M., and KONDOW, T., 1995, *J. chem. Phys.*, **102**, 5960.
[18] GANTEFÖR, G., GAUSA, M., MEIWES-BROER, K.-H., and LUTZ, H. O., 1990, *J. chem. Soc., Faraday Trans.*, **86**, 2483.
[19] TAYLOR, K. J., PETTIETTE-HALL, C. L., CHESHNOVSKY, O., and SMALLEY, R. E., 1992, *J. chem. Phys.*, **96**, 3319.
[20] WANG, L.-S., and WU, H., 1998, *Advances in Metal and Semiconductor Clusters*, Vol. 4, edited by Michael A. Duncan (Greenwich, Connecticut: JAI), p. 299.
[21] HANLEY, L., RUATTA, S. A., and ANDERSON, S. L., 1987, *J. chem. Phys.*, **87**, 260.
[22] RAY, U., and JARROLD, M. F., 1993, *Advances in Metal and Semiconductor Clusters*, Vol. 1, edited by M. A. Duncan (Greenwich, Connecticut: JAI), p. 1.
[23] ARMENTROUT, P. B., HALES, D. A., and LIAN, L., 1994, *Advances in Metal and Semiconductor Clusters*, Vol. 2, edited by M. A. Duncan (Greenwich, Connecticut: JAI, p. 1.
[24] KRÜCKEBERG, S., DIETRICH, L., LÜTZENKIRCHEN, K., SCHWEIKHARD, L., WALTHER, C., and ZIEGLER, J., 1999, *J. chem. Phys.*, **110**, 7216.
[25] SPASOV, V. A., LEE, T.-H., MABERRY, J. P., and ERVIN, K. M., 1999, *J. chem. Phys.*, **110**, 5208.
[26] ALONSO, J. A., 2000, *Chem. Rev.*, **100**, 637.
[27] PARENT, D. C., and ANDERSON, S. L., 1992, *Chem. Rev.*, **92**, 1541.
[28] MITCHELL, S. A., LIAN, L., RAYNER, D. M., and HACKETT, P. A., 1995, *J. chem. Phys.*, **103**, 5539.
[29] MITCHELL, S. A., RAYNER, D. M., BARTLETT, T., and HACKETT, P. A., 1996, *J. chem. Phys.*, **104**, 4012.
[30] ARMENTROUT, P. B., 1996, *Metal–Ligand Interactions—Structure and Reactivity*, edited by N. Russo and D. R. Salahub (Dordrecht: Kluwer), p. 23.
[31] COX, D. M., KALDOR, A., FAYET, P., EBERHARDT, W., BRICKMAN, R., SHERWOOD, R., FU, Z., and SONDERICHER, D., 1990, *Novel Materials in Heterogeneous Catalysis*, edited by R. T. K. Baker, and L. L. Murrell (Washington, DC: American Chemical Society), p. 172.
[32] XU, J., RODGERS, M. T., GRIFFIN, J. B., and ARMENTROUT, P. B., 1998, *J. chem. Phys.*, **108**, 9339.
[33] BERG, C., BEYER, M., ACHATZ, U., JOOS, S., NIEDNER-SCHATTEBURG, G., and BONDYBEY, V. E., 1998, *J. chem. Phys.*, **108**, 5398.
[34] BOWERS, M. T., KEMPER, P. R., VAN KOPPEN, P., WYTTENBACH, T., CARPENTER, C. J., WEIS, P., and GIDDEN, J., 1999, *Energetics of Stable Molecules and Reactive Intermediates*, edited by M. E. Minas de Piedade (Dordrecht: Kluwer), p. 235.
[35] VANN, W. D., and CASTLEMAN, A. W., JR, 1999, *J. phys. Chem.* A, **103**, 847.
[36] JIAO, C. Q., RANATUNGA, D. R., and FREISER, B. S., 1996, *J. phys. Chem.*, **100**, 4755.
[37] LAFLEUR, R. D., PARNIS, J. M., and RAYNER, D. M., 1996, *J. chem. Phys.*, **105**, 3551.
[38] GEHRET, O., and IRION, M. P., 1996, *Chem. Phys. Lett.*, **254**, 379.
[39] KURIKAWA, T., HIRANO, M., TAKEDA, H., YAGI, K., HOSHINO, K., NAKAJIMA, A., and KAYA, K., 1995, *J. phys. Chem.*, **99**, 16248.
[40] BÉRCES,. A., HACKETT, P. A., LIAN, L., MITCHELL, S. A., and RAYNER, D. M., 1998, *J. chem. Phys.*, **108**, 5476.
[41] PEDERSEN, D. B., PARNIS, J. M., and RAYNER, D. M., 1998, *J. chem. Phys.*, **109**, 551.

[42] RIDGE, D. P., 1994, *Unimolecular and Bimolecular Reaction Dynamics*, edited by C.-Y. Ng, T. Baer and I. Powis (New York: Wiley), p. 337.
[43] HOLMGREN, L., and ROSÉN, A., 1999, *J. chem. Phys.*, **110**, 2629.
[44] DIETRICH, G., DASGUPTA, K., LÜTZENKIRCHEN, K., SCHWEIKHARD, L., and ZIEGLER, J., 1996, *Chem. Phys. Lett.*, **252**, 141.
[45] MIKHAILOV, V. A., BARRAN, P. E., and STACE, A. J., 1999, *Phys. Chem. chem. Phys.*, **1**, 3461.
[46] FEDRIGO, S., HASLETT, T. L., and MOSKOVITS, M., 1999, *Chem. Phys. Lett.*, **307**, 333.
[47] PARKS, E. K., KERNS, K. P., and RILEY, S. J., 2000, *J. chem. Phys.*, **112**, 3384.
[48] PARKS, E. K., KERNS, K. P., and RILEY, S. J., 2000, *J. chem. Phys.*, **112**, 3394.
[49] WÖSTE, L., 1996, *Z. phys. Chem.* (*Munich*), **196**, 1.
[50] KNICKELBEIN, M. B., 1999, *Phil. Mag.* B, **79**, 1379.
[51] YANG, D.-S., ZGIERSKI, M. Z., RAYNER, D. M., HACKETT, P. A., MARTINEZ, A., SALAHUB, D. R., ROY, P.-N., and CARRINGTON, T., JR, 1995, *J. chem. Phys.*, **103**, 5335.
[52] YANG, D.-S., ZGIERSKI, M. Z., BÉRCES, A., HACKETT, P. A., MARTINEZ, A., and SALAHUB, D. R., 1997, *Chem. Phys. Lett.*, **227**, 71.
[53] YANG, D.-S., ZGIERSKI, M. Z., BÉRCES, A., and HACKETT, P. A., 1996, *J. chem. Phys.*, **105**, 10663.
[54] HASLETT, T. L., BOSNICK, K. A., and MOSKOVITS, M., 1998, *J. chem. Phys.*, **108**, 3453.
[55] BOSNICK, K. A., HASLETT, T. L., FEDRIGO, S., MOSKOVITS, M., CHAN, W.-T., and FOURNIER, R., 1999, *J. chem. Phys.*, **111**, 8867.
[56] JACKSON, K. A., KNICKELBEIN, M., KORETSKY, G., and SRINIVAS, S., 2000, *Chem. Phys.*, **262**, 41.
[57] DIETRICH, G., KRÜCKEBERG, S., LÜTZENKIRCHEN, K., SCHWEIKHARD, L., and WALTHER, C., 2000, *J. chem. Phys.*, **112**, 752.
[58] JELLINEK, J. (editor), 1999, *Theory of Atomic and Molecular Clusters* (Berlin: Springer).
[59] KAPILOFF, E., and ERVIN, K. M., 1997, *J. phys. Chem.* A, **101**, 8460.
[60] GUO, B. C., KERNS, K. P., and CASTLEMAN, A. W., JR, 1992, *J. chem. Phys.*, **96**, 8177.
[61] KORETSKY, G. M., KERNS, K. P., NIEMAN, G. C., KNICKELBEIN, M. B., and RILEY, S. J., 1999, *J. phys. Chem.* A, **103**, 1997.
[62] BRECHIGNAC, C., BRECHNIGNAC, P., FAYET, P., SAUNDERS, W. A., and WOSTE, L., 1988, *J. chem. Phys.*, **89**, 2419.
[63] MINGOS, D. M. P., and WALES, D. J., 1990, *J. Am. chem. Soc.*, **112**, 930.
[64] PARKS, E. K., ZHU, L., HO, J., and RILEY, S. J., 1993, *Z. Phys.* D, **26**, 41.
[65] DUNCAN, M. A., 1993–1998, *Advances in Metal and Semiconductor Clusters*, Vols 1–4 (Greenwich, Connecticut: JAI).
[66] MOSKOVITS, M., 1991, *A. Rev. phys. Chem.*, **42**, 465.
[67] MORSE, M. D., 1986, *Chem. Rev.*, **86**, 1049.
[68] RILEY, S. J., 1992, *Metal–Ligand Interactions: From Atoms to Clusters to Surfaces*, edited by D. R. Salahub and N. Russo (Dordrecht: Kluwer), p. 17.
[69] RILEY, S. J., 1992, *Ber. Bunsenges. phys. Chem.*, **96**, 1104.
[70] CASTLEMAN, A. W., JR, HARMS, A. C., and LEUCHTNER, R. E., 1991, *Z. Phys.* D, **19**, 343.
[71] SCHMID, G., BÄUMLE, M., GEERKENS, M., HEIM, I., OSEMANN, C., and SAWITOWSKI, T., 1999, *Chem. Soc. Rev.*, **28**, 179.
[72] AIKEN, J. D., III, and FINKE, R. G., 1999, *J. molec. Catal.* A, **145**, 1.
[73] KNICKELBEIN, M. B., 1999, *A. Rev. phys. Chem.*, **50**, 79.
[74] KALDOR, A., COX, D. M., TREVOR, D. J., and ZAKIN, M. R., 1986, *Z. Phys.* D, **3**, 195.
[75] ARMENTROUT, P. B., and KICKEL, B. L., 1996, *Organometallic Ion Chemistry*, edited by B. S. Freiser (Dordrecht: Kluwer), p. 1.
[76] MORSE, M. D., 1993, *Advances in Metal and Semiconductor Clusters*, Vol. 1 edited by M. A. Duncan (Greenwich, CT: JAI), p. 83.
[77] SOMORJAI, G. A., 1981, *Chemistry in Two Dimensions: Surfaces* (Ithaca, New York: Cornell University Press).
[78] KISKINOVA, M., 1991, *Stud. Surf. Sci. Catal.* **64**, 37.
[79] CONNOR, J. A., 1997, *Inorganic Chemistry: Metal Carbonyl Chemistry*, Topics in Current Chemistry, Vol. 71 (Berlin: Springer), p. 71.
[80] KHARA, K. C., and DAHL, L. F., 1988, *Adv. chem. Phys.*, **70**, 1.
[81] FARRUGIA, L. J., 1997, *J. chem. Soc., Dalton Trans.*, 1783.

[82] Hughes, A. K., and Wad, K., 2000, *Coord. Chemistry Rev.*, **197**, 191.
[83] Heck, R. M., and Farrauto, R. J., 1995, *Catalytic Air Pollution Control: Commercial Technology* (New York: Van Nostrand Reinhold).
[84] Frenking, G., and Fröhlich, N., 2000, *Chem. Rev.*, **100**, 717.
[85] Dedieu, A., 2000, *Chem. Rev.*, **100**, 543.
[86] Blyholder, G., 1964, *J. phys. Chem.*, **68**, 2772.
[87] Maruyama, S., Anderson, L. R., and Smalley, R. E., 1990, *Rev. scient. Instrum.*, **61**, 3686.
[88] Milani, P., and DeHeer, W. A., 1990, *Rev. scient. Instrum.*, **61**, 1835.
[89] Loh, S. K., Hales, D. A., and Armentrout, P. B., 1986, *Chem. Phys. Lett.*, **129**, 527.
[90] Vann, W. D., Wagner, R. L., and Castleman, A. W., jr, 1998, *J. phys. Chem.* A, **102**, 1708.
[91] Jiao, C. Q., and Freiser, B. S., 1995, *J. phys. Chem.*, **99**, 10723.
[92] Rohlfing, E. A., Cox, D. M., and Kaldor, A., 1983, *Chem. Phys. Lett.*, **99**, 161.
[93] Fayet, P., and Wöste, L., 1985, *Surf. Sci.*, **156**, 134.
[94] Magnera, T., David, D. E., and Michl, J., 1987, *J. Am. chem. Soc.*, **109,** 936.
[95] Freiser, B. S., 1996, *J. mass Spectrom.*, **31**, 703.
[96] Meiwes-Broer, K. H., 1992, *Appl. Phys.* A, **55**, 430.
[97] Siekmann, H. R., Lüder, C., Faehrmann, J., Lutz, H. O., and Mewies-Broer, K. H., 1991, *Z. Phys.* D, **20**, 417.
[98] Lu, W., Huang, R., Ding, J., and Yang, S., 1996, *J. chem. Phys.*, **104**, 6577.
[99] Ren, X., Hintz, P. A., and Ervin, K. M., 1993, *J. chem. Phys.*, **99**, 3575.
[100] Leopold, D. G., Ho, J., and Lineberger, W. C., 1987, *J. chem. Phys.*, **86**, 1715.
[101] Ho, J., Evans, K. M., and Lineberger, W. C., 1990, *J. chem. Phys.*, **93**, 6987.
[102] Casey, S. M., and Leopold, D. G., 1993, *Chem. Phys. Lett.*, **201**, 205.
[103] Schultz, R. H., Crellin, K. C., and Armentrout, P. B., 1991, *J. Am. chem. Soc.*, **113**, 8590.
[104] Armentrout, P. B., University of Utah, private communication.
[105] Yamada, Y., and Castleman, A. W., Jr, 1992, *J. chem. Phys.*, **97**, 4543.
[106] Klots, T. D., Winter, B. J., Parks, E. K., and Riley, S. J., 1990, *J. chem. Phys.*, **92**, 2110.
[107] Cohen, M. L., Chou, M. Y., Knight, W. D., and de Heer, W. A., 1987, *J. phys. Chem.*, **91**, 3141.
[108] Brack, M., 1993, *Rev. mod. Phys.*, **65**, 677.
[109] deHeer, W., 1993, *Rev. mod. Phys.*, **65**, 611.
[110] Kroto, H. W., Heath, J. R., O'Brien, S. C., Curl, R. F., and Smalley, R. E., 1985, *Nature*, **318**, 162.
[111] Hunter, J. M., Fye, J. L., Jarrold, M. F., and Bower, J. E., 1994, *Phys. Rev. Lett.*, **73**, 2063.
[112] Hamrick, Y., Taylor, S., Lemire, G. W., Fu, Z.-W., Shui, J.-C., and Morse, M. D., 1988, *J. chem. Phys.*, **88**, 4095.
[113] Knickelbein, M. B., and Yang, S., 1990, *J. chem. Phys.*, **93**, 1476.
[114] Shi, Y., Spasov, V. A., and Ervin, K. M., 2001, *Int. J. mass Spectrom.* **205** (in the press).
[115] Lee, T. H., and Ervin, K. M., 1994, *J. phys. Chem.*, **98**, 10023.
[116] Powers, D. E., Hansen, S. G., Geusic, M. E., Michalopoulos, D. L., and Smalley, R. E., 1983, *J. chem. Phys.*, **78**, 2866.
[117] Alameddin, G., Hunter, J., Cameron, D., and Kappes, M. M., 1992, *Chem. Phys. Lett.*, **192**, 122.
[118] Knickelbein, M. B., 1992, *Chem. Phys. Lett.*, **192,** 129.
[119] Jackschath, C., Rabin, I., and Schulze, W., 1992, *Z. Phys.* D, **22**, 517.
[120] Becker, S., Dietrich, G., Hasse, H-U., Klisch, N., Kluge, H.-J., Kreisle, K., Krückeberg, S., Lindinge, M., Lützenkirchen, K., Schweikhard, L., Weidele, H., and Ziegler, J., 1994, *Z. Phys.* D, **30**, 341.
[121] Krückeberg, S., Dietrich, G., Lützenkirchen, K., Schweikhard, L., Walther, C., and Ziegler, J., 1996, *Int. J. mass Spectrom. ion Processes*, **155**, 141.
[122] Hild, U., Dietrich, G., Krückeberg, S., Lindinger, M., Lützenkirchen, K., Schwikhard, L., Walther, C., and Ziegler, J., 1998, *Phys. Rev.* A, **57**, 2786.
[123] Shi, Y., Spasov, V. A., and Ervin, K. M., 1999, *J. chem. Phys.*, **111**, 938.

[124] Spasov, V. A., Lee, T.-H., and Ervin, K. M., 2000, *J. chem. Phys.*, **112**, 1713.
[125] Spasov, V. A., Shi, Y., and Ervin, K. M., 2000, *Chem. Phys.*, **262**, 75.
[126] Taylor, K. J., Jin, C., Conceicao, J., Wang, L. S., Chesnovsky, O., Johnson, B. R., Nordlander, P. J., and Smalley, R. E., 1990, *J. chem. Phys.*, **93**, 7515.
[127] Balasubramanian, K., and Liao, D.-W., 1991, *J. chem. Phys.*, **94**, 5233.
[128] Gantefor, G. F., Cox, D. M., and Kaldor, A., 1992, *J. chem. Phys.*, **96**, 4102.
[129] Häkkinen, H., and Landman, U., 2000, *Phys. Rev.* B, **62**, R2287.
[130] Cox, D. M., Reichmann, K. C., Trevor, D. J., and Kaldor, A., 1988, *J. chem. Phys.*, **88**, 111.
[131] Leuchtner, R. E., Harms, A. C., and Castleman, A. W., Jr, 1990, *J. chem. Phys.*, **92**, 6527.
[132] Alford, J. M., Weiss, F. D., Laaksonen, R. T., and Smalley, R. E., 1986, *J. phys. Chem.*, **90**, 4480.
[133] Armentrout, P. B., and Clemmer, D. E., 1992, *Energetics of Organometallic Species*, edited by J. A. Martinho Simões (Dordrecht: Kluwer), p. 321.
[134] Graul, S. T., and Squires, R. R., 1988, *Mass Spectrom. Rev.*, **7**, 263.
[135] Hintz, P. A., and Ervin, K. M., 1994, *J. chem. Phys.*, **100**, 5715.
[136] Mwakapumba, J., and Ervin, K. M., 1997, *Int. J. mass Spectrom. ion Processes*, **161**, 161.
[137] Hintz, P. A., and Ervin, K. M., 1995, *J. chem. Phys.*, **103**, 7897.
[138] Grushow, A., and Ervin, K. M., 1995, *J. Am. chem. Soc.*, **117**, 11612.
[139] Harris, J., and Luntz, A. C., 1989, *J. chem. Phys.*, **91**, 6421.
[140] Wang, Y. W., Lin, J. C., and Engel, T., 1993, *Surf. Sci.*, **289**, 267.
[141] D'Evelyn, M. P., Steinbrück, H. P., and Madix, R. J., 1987, *Surf. Sci.*, **180**, 47.
[142] Lian, L., Hackett, P. A., and Rayner, D. M., 1993, *J. chem. Phys.*, **99**, 2583.
[143] Armentrout, P. B., and Simons, J., 1992, *J. Am. chem. Soc.*, **114**, 8627.
[144] Darling, J. H., and Ogden, J. S., 1972, *Inorg. Chem.*, **11**, 666.
[145] Libuda, J., Sandell, A., Bäumer, M., and Freund, H.-J., 1995, *Chem. Phys. Lett.*, **240**, 429.
[146] Dixon, K. R., and Dixon, A. C., 1995, *Comprehensive Organometallic Chemistry II*, Vol. 9 edited by R. J. Puddephatt (Oxford: Pergamon), p. 198.
[147] Yeo, Y. Y., Vattuone, L., and King, D. A., 1997, *J. chem. Phys.*, **106**, 1990.
[148] Parks, E. K., Nieman, G. C., Pobo, L. G., and Riley, S. J., 1988, *J. chem. Phys.*, **88**, 6260.
[149] Parks, E. K., Winter, B. J., Klots, T. D., and Riley, S. J., 1991, *J. chem. Phys.*, **94**, 1882.
[150] Klots, T. D., Winter, B. J., Parks, E. K., and Riley, S. J., 1991, *J. chem. Phys.*, **95**, 8919.
[151] Winter, B. J., Klots, T. D., Parks, E. K., and Riley, S. J., 1991, *Z. Phys.* D, **19**, 375.
[152] Parks, E. K., Winter, B. J., Klots, T. D., and Riley, S. J., 1992, *J. chem. Phys.*, **96**, 8267.
[153] Parks, E. K., Klots, T. D., Winter, B. J., and Riley, S. J., 1993, *J. chem. Phys.*, **99**, 5831.
[154] Parks, E. K., Zhu, L., Ho, J., and Riley, S. J., 1994, *J. chem. Phys.*, **100**, 7206.
[155] Parks, E. K., Zhu, L., Ho, J., and Riley, S. J., 1995, *J. chem. Phys.*, **102**, 7377.
[156] Ho, J., Parks, E. K., Zhu, L., and Riley, S. J., 1995, *Chem. Phys.*, **201**, 245.
[157] Parks, E. K., and Riley, S. J., 1995, *Z. Phys.* D, **33**, 59.
[158] Parks, E. K., Nieman, G. C., Kerns, K. P., and Riley, S. J., 1997, *J. chem. Phys.*, **107**, 1861.
[159] Parks, E. K., Kerns, K. P., and Riley, S. J., 1998, *J. chem. Phys.*, **109**, 10207.
[160] Guo, B. C., Kerns, K. P., and Castleman, A. W., Jr, 1992, *J. phys. Chem.*, **96**, 6931.
[161] Fayet, P., McGlinchey, M. J., and Wöste, L., 1987, *J. Am. chem. Soc.*, **109**, 1733.
[162] Vajda, S., Leisner, T., Wolf, S., and Wöste, L. H., 1999, *Phil. Mag.* B, **79**, 1353.
[163] Teo, B. K., 1984, *Inorg. Chem.*, **23**, 1251.
[164] Teo, B. K., Longoni, G., and Chung, F. R. K., 1984, *Inorg. Chem.*, **23**, 1257.
[165] Teo, B. K., 1985, *Inorg. Chem.*, **24**, 4209.
[166] Evans, D. G., and Mingos, M. P., 1982, *J. organometall. Chem.*, **240**, 321.
[167] Mingos, D. P., 1985, *J. chem. Soc., chem. Commun.*, 1352.

[168] MINGOS, D. P., 1985, *Inorg. Chem.*, **24**, 114.
[169] OWEN, S. M., 1988, *Polyhedron*, **7**, 253.
[170] PARKS, E. K., NIEMAN, G. C., and RILEY, S. J., 1996, *Surf. Sci.*, **355**, 127.
[171] PARKS, E. K., NIEMAN, G. C., KERNS, K. P., and RILEY, S. J., 1998, *J. chem. Phys.*, **108**, 3731.
[172] CONCEIÇÃO, J., LOH, S. K., LIAN, L., and ARMENTROUT, P. B., 1996, *J. chem. Phys.*, **104**, 3976.
[173] PARKS, E. K., and RILEY, S. J., 1993, *J. chem. Phys.*, **99**, 5898.
[174] GRUSHOW, A., and ERVIN, K. M., 1997, *J. chem. Phys.*, **106**, 9580.
[175] SPASOV, V. A., and ERVIN, K. M., 1998, *J. chem. Phys.*, **109**, 5344.
[176] DETURI, V. F., HINTZ, P. A., and ERVIN, K. M., 1997, *J. phys. Chem.* A, **101**, 5969.
[177] GERLICH, D., 1992, *Adv. chem. Phys.*, **82**, 1.
[178] ERVIN, K. M., and ARMENTROUT, P. B., 1985, *J. chem. Phys.*, **83**, 166.
[179] RODGERS, M. T., ERVIN, K. M., and ARMENTROUT, P. B., 1997, *J. chem. Phys.*, **106**, 4499.
[180] RODGERS, M. T., and ARMENTROUT, P. B., 1998, *J. chem. Phys.*, **109**, 1787.
[181] ARMENTROUT, P. B., 2000, *Int. J. Mass Spectrom.*, **200**, 219.
[182] ARMENTROUT, P. B., 1992, *Advances in Gas Phase Ion Chemistry*, Vol. 1, edited by N. G. Adams and L. M. Babcock (Greenwich, Connecticut: JAI), p. 83.
[183] ARMENTROUT, P. B., and ERVIN, K. M., 2000, CRUNCH, Fortran program (University of Utah, Salt Lake City; University of Nevada, Reno).
[184] DALLESKA, N. F., HONMA, K., SUNDERLIN, L. S., and ARMENTROUT, P. B., 1994, *J. Am. chem. Soc.*, **116**, 3519.
[185] SUNDERLIN, L. S., WANG, D., and SQUIRES, R. R., 1993, *J. Am. chem. Soc.*, **115**, 12060.
[186] SIEVERS, M. R., and ARMENTROUT, P. B., 1995, *J. phys. Chem.*, **99**, 8135.
[187] KHAN, F. A., STEELE, D. A., and ARMENTROUT, P. B., 1995, *J. phys. Chem.*, **99**, 7819.
[188] FERGUSON, E. E., 1983, *Chem. Phys. Lett.*, **99**, 89.
[189] SIEVERS, M. R., CHEN, Y.-M., and ARMENTROUT, P. B., 1996, *J. chem. Phys.*, **105**, 6322.
[190] BURLEY, J. D., ERVIN, K. M., and ARMENTROUT, P. B., 1987, *J. chem. Phys.*, **86**, 1944.
[191] ERVIN, K. M., and ARMENTROUT, P. B., 1987, *J. chem. Phys.*, **86**, 6240.
[192] ERVIN, K. M., and ARMENTROUT, P. B., 1989, *J. chem. Phys.*, **90**, 118.
[193] TAYLOR, S., LEMIRE, G. W., HAMRICK, Y. M., FU, Z., and MORSE, M. D., 1988, *J. chem. Phys.*, **89**, 5517.
[194] PINEGAR, J. C., LANGENBERG, J. D., ARRINGTON, C. A., SPAIN, E. M., and MORSE, M. D., 1995, *J. chem. Phys.*, **102**, 666.
[195] LANGENBERG, J. D., and MORSE, M. D., 1998, *J. chem. Phys.*, **108**, 2331.
[196] RUSSON, L. M., HEIDECKE, S. A., BIRKE, M. K., CONCEICAO, J., MORSE, M. D., and ARMENTROUT, P. B., 1994, *J. chem. Phys.*, **100**, 4747.
[197] SIMARD, B., LEBEAULT-DORGET, M.-A., MARIJNISSEN, A., and TER MEULEN, J. J., 1998, *J. chem. Phys.*, **108**, 9668.
[198] HOLMGREN, L., GRÖNBECK, H., ANDERSSON, M., and ROSÉN, A., *Phys. Rev.* B, **53**, 16611.
[199] NYGREN, M. A., SIEGBAHN, P. E., JIN, C., GUO, T., and SMALLEY, R. E., 1991, *J. chem. Phys.*, **95**, 6181.
[200] LONGONI, G., and CHINI, P., 1976, *J. Am. chem. Soc.*, **98**, 7725.
[201] LONGONI, G., CHINI, P., and CAVALIERI, A., 1976, *Inorg. Chem.*, **15**, 3025.
[202] COTTON, F. A., and WILKINSON, G., 1988, *Advanced Inorganic Chemistry*, fifth edition (New York: Wiley).
[203] MEALLI, C., 1985, *J. Am. chem. Soc.*, **107**, 2245.
[204] EVANS, D. G., 1988, *J. organometall. Chem.*, **352**, 397.
[205] ROSZAK, S., and BALASUBRAMANIAN, K., 1995, *J. chem. Phys.*, **103**, 1043.
[206] GRÖNBECK, H., and ANDREONI, W., 1997, *Chem. Phys. Lett.*, **269**, 385.
[207] SCHULZE ICKING-KONERT, G., HANDSCHUH, H., GANTEFÖR, G., and EBERHARDT, W., 1996, *Phys. Rev. Lett.*, **76**, 1047.
[208] GANTEFÖR, G., SCHULZE ICKING-KONERT, G., HANDSCHUH, H., and EBERHARDT, W., 1996, *Int. J. Mass. Spectrom. Ion Processes*, **159**, 81.
[209] ANDERSON, A., and AWARD, M. K., 1985, *J. Am. chem. Soc.*, **107**, 7854.
[210] SZANYI, J., KUHN, W. K., and GOODMAN, D. W., 1993, *J. vac. Sci. Technol.* **11**, 1969.
[211] BLOMBERG, M. R. A., LEBRILLA, C. B., and SIEGBAHN, P. E. M., 1988, *Chem. Phys. Lett.*, **150**, 522.

[212] DAI, D., ROSZAK, S., and BALASUBRAMANIAN, K., 1996, *J. chem. Phys.*, **104**, 1471.
[213] JARROLD, M. F., ILLIES, A. J., and BOWERS, M. T., 1985, *J. Am. chem. Soc.*, **107**, 7339.
[214] RAY, U., JARROLD, M. F., BOWER, J. E., and KRAUS, J. S., 1989, *J. chem. Phys.*, **91**, 2912.
[215] HAUPT, S., KALLER, J., SCHOOS, D., CAMERON, D., and KAPPES, M. M., 1997, *Z. Phys.* D, **40**, 331.
[216] DIETRICH, G., DASGUPTA, K., KRÜCKEBERG, S., LÜTZENKIRCHEN, K., SCHWEIKHARD, L., WALTHER, C., and ZIEGLER, J., 1996, *Chem. Phys. Lett.*, **250**, 397.
[217] WALTHER, C., DIETRICH, G., LINDINGER, M., LÜTZENKIRCHEN, K., SCHWEIKHARD, L., and ZIEGLER, J., 1996, *Chem. Phys. Lett.*, **256**, 77.
[218] SCHWIKHARD, L., DIETRICH, G., HILD, U., KRÜCKEBERG, S., LÜTZENKIRCHEN, K., and WALTHER, C., 1997, *Rapid Commun. mass Spectrom.*, **11**, 1624.
[219] LINDINGER, M., DASGUPTA, K., DIETRICH, G., KRÜCKEBERG, S., KUZNETSOV, S., LÜTZENKIRCHEN, K., SCHWEIKHARD, L., WALTHER, C., and ZIEGLER, J., 1997, *Z. Phys.* D, **40**, 347.
[220] HUSBAND, J., AGUIRRE, F., THOMPSON, C. J., LAPERLE, C. M., and METZ, R. B., 2000, *J. Phys. Chem.* A, **104**, 2020.
[221] AGUIRRE, F., HUSBAND, J., THOMPSON, C. J., and METZ, R., 2000, *Chem. Phys. Lett.*, **318**, 466.
[222] HUANG, F.-S., and DUNBAR, R. C., 1991, *Int. J. mass Spectrom. ion Processes*, **109**, 151.
[223] HO, Y.-P., DUNBAR, R. C., and LIFSHITZ, C., 1995, *J. Am. chem. Soc.*, **117**, 6504.
[224] GILBERT, R. G., and SMITH, S. C., 1990, *Theory of Unimolecular and Recombination Reactions* (Boston: Blackwell Scientific).
[225] BAER, T., and HASE, W. L., 1996, *Unimolecular Reaction Dynamics: Theory and Experiments* (New York: Oxford University Press).
[226] DETURI, V. F., and ERVIN, K. M., 1999, *J. phys. Chem.* A, **103**, 6911.
[227] SHVARTSBURG, A. A., ERVIN, K. M., and FREDERICK, J. H., 1996, *J. chem. Phys.*, **104**, 8458.
[228] KAPPES, M. M., and STALEY, R. H., 1981, *J. Am. chem. Soc.*, **103**, 1286.
[229] WESENDRUP, R., and SCHWARZ, H., 1997, *Organometallics*, **16**, 461.
[230] PAVLOV, M., BLOMBERG, M. R. A., SIEGBAHN, P. E. M., WESENDRUP, R., HEINEMANN, C., and SCHWARZ, H., 1997, *J. phys. Chem.* A, **101**, 1567.
[231] BERG, C., KAISER, S., SCHINDLER, T., KRONSEDER, C., NIEDNER-SCHATTEBURG, G., and BONDYBEY, V. E., 1994, *Chem. Phys. Lett.*, **231**, 139.
[232] SIEVERS, M. R., and ARMENTROUT, P. B., 1999, *Int. J. mass Spectrom.*, **185–187**, 117.
[233] CAMPBELL, I. M., 1988, *Catalysis at Surfaces* (London: Chapman & Hall).
[234] ADAMSON, A. W., and GAST, A. P., 1997, *Physical Chemistry of Surfaces* (New York: Wiley).
[235] SAULT, A. G., and GOODMAN, D. W., 1989, *Adv. chem. Phys.*, **76**, 153.
[236] BERNASEK, S. L., 1995, *Heterogeneous Reaction Dynamics* (New York: VCH).
[237] LIU, Z. M., ZHOU, Y., SOLYMOSI, F., and WHITE, J. M., 1991, *Surf. Sci.* **245**, 289.
[238] SHI, Y., DOGBEVIA, M., and ERVIN, K. M., 2000, unpublished.